PROBING THE CANCER GLYCOCALYX WITH HIGH-CONTENT RESOLUTION

A Thesis

Presented to the Faculty of the Graduate School

of Cornell University

In Partial Fulfillment of the Requirements for the Degree of

Master of Science

by

Richard Huang

May 2023

ABSTRACT

Glycocalyx refers to the outermost layer or sugar cell coat of many cells, which consists of glycoproteins, glycolipids, and glycoRNAs. It often plays a critical role in many biological processes, such as mediating immune responses and intercellular communications. The drastically altered glycosylation pattern in cancer cells, which results in a different sugar coat than healthy cells, has been observed for decades. It has been demonstrated to be correlated with tumor growth, proliferation, invasion, metastasis, and immunity. A comprehensive understanding of the glycocalyx differences between healthy cells and cancerous cells will be instrumental for the development of faster and more effective cancer diagnoses and therapies. We envisioned to incorporate advanced high-resolution microscopy and glycan-binding protein engineering for better imaging techniques in studying cancer-associated cell surface glycans. This thesis summarizes in detail our recent advancements in developing a molecular toolkit suitable for cell surface glycan imaging with expansion microscopy. In this toolkit, engineered glycan-binding proteins are selected as probes for glycan imaging to achieve structural specificity. Sortase-mediated transpeptidation is used as a versatile, site-specific protein modification method that can be used for different kinds of glycan-binding proteins, including carbohydrate-binding modules (CBMs) and adaptive immune proteins, while maintaining their binding affinities and specificities.

BIOGRAPHICAL SKETCH

Richard Yuding Huang was born in Changsha, China, in 1998. He received his training in Organic Chemistry from Harvard University in 2019 and his bachelor's degree in Materials Chemistry from Central South University in 2020. In 2021, he joined the DeLisa Research Group at Cornell University to work on his M.S. thesis with the mentorship of Prof. Matthew DeLisa and Dr. Jinjoo Jung. His research interests include Bioorganic Chemistry, Chemical Biology, and Immunology, and his research mission statement is to use chemistry and chemical tools to gain a better understanding of human diseases and provide insights into more efficient future diagnostics and therapeutics. After completing his M.S. Program at Cornell, Richard plans to continue his academic career in a Ph.D. program in Chemistry and Chemical Biology. In additional to research, Richard dedicates part of his extra time to promoting the value of diversity, equity, and inclusion in academia and scientific community. He is the Depute Coordinator of Diversity and Inclusion Program (DIP) in the Chemical and Biomolecular Engineering School at Cornell, as well as the Graduate Lead in Cornell Asian and Asian American Center (A3C). Apart from science, Richard loves music and art. He is an amateur violinist, a classical music enthusiast, and a fan of Impressionism painting.

This work is dedicated to all those who suffer from cancer and their loved ones.

ACKNOWLEDGMENTS

I would like to express my sincere gratitude to all those who have helped, supported, and loved me, bringing me to where I am today, which has not been an easy journey. First and foremost, my parents and grandparents, who have done their best to provide love and support to the best of their understanding and abilities. I am especially grateful for the emotional and financial support my parents offered, without which pursuing my studies abroad would have been much harder. I also want to acknowledge my high school chemistry teacher, Mr. Xie, who introduced me to the magical world of chemistry that I have been in love with ever since.

At Cornell, I feel tremendously fortunate to have gotten to know and interact with a group of inspirational, intelligent, and affable professors and cohorts. Although I was trained as a synthetic chemist, I decided to be re-trained as a chemical biologist. Thanks to all these people, this adventure has become smoother and more joyful. I greatly appreciate Prof. Matthew DeLisa, who warmly welcomed me to the DeLisa Research Group and provided me with precious mentorship all along the way. I thank him for trusting me on this research project, from which I gained a rich experience. I appreciate the help and mentorship from Dr. Jinjoo Jung, one of the postdocs in the DeLisa Research Group and a talented chemical biologist, from whom I have learnt a lot about chemical biology research. We always had great times in the lab, even when facing the setbacks in our research. I would like to acknowledge Prof. Matthew Paszek and Prof. Christopher Alabi, who are the collaborators on this project and made it possible for me to learn from people with different academic backgrounds. I also want to express my sincere gratitude to Prof. Jeremy Baskin, who inspired, encouraged, and helped me to continue my scientific career as a chemical biologist. I thank him for all his support for

my M.S. program here at Cornell and my pursue of Ph.D. program. It is my great pleasure to have both him and Prof. Paszek on the special committee for my M.S. thesis work. Additionally, I would like to thank Dr. Beth Rhoades for inspiring my interest in immunology, which helped me understand my research better and will surely help me in my future career. I thank Natalia, who is also graduating this year with a Ph.D. degree from the DeLisa Research Group at Cornell, for helping me with all the extra training in research and giving me great advice concerning my Ph.D. application and scientific career. Moreover, I want to express my great appreciation to my friends here at Cornell, including Reeby, Mavis, Allison, Ayo, Daniel, Belen, Brain and more, for being there for me all the time, giving me patience in the tough times and joy in the down times, and most importantly, helping me understand myself better.

Last but not least, I would love to thank the United States of America for continually opening her doors for me and the people like me, and for giving me the opportunities to be myself and pursue the life I aspired to have. When I first came to this country in 2019, I immediately and strangely felt at home. Back then, I was on the edge of abandoning my scientific career, but thankfully, the free, vibrant, and independent academic atmosphere here helped me fall back in love with science again and convinced me to continue pursuing a career in academia.

TABLE OF CONTENTS

LIST OF FIGURES

LIST OF TABLES

PREFACE

This thesis will be focusing on the work I have done in a collaborative project called GlycoExM, which was co-developed by Prof. DeLisa, Prof. Paszek, and Prof. Alabi in the Chemical and Biomolecular Engineering School at Cornell. GlycoExM aims to utilize the most advanced techniques in biophysics, immunology, and biomolecular engineering to achieve the high-content resolution imaging of cell surface glycans. We aspire to use glycan-binding proteins, including carbohydrate-binding modules (CBMs) and adaptive immune proteins, for their structural and sequential glycan specificity, and to use expansion microscopy for high-content resolution of the crowded cell surface glycans, especially those on cancer cells. My role in this project is to optimize the glycan-binding protein library and their modification methods, and also to test the binding affinity and the specificity of these selected engineered proteins. In this thesis, I will also provide the biological and clinical background of this technique, as well as the future direction of this project.

I. Backgrounds and Introductions

1. Cancer Diagnostics and Therapeutics

Cancer is the second leading cause of death in the United States and a major public health problem in the world. In 2023, it is estimated that 1,958,310 new cancer cases and 609,820 cancer deaths will occur in the United States (1). Detecting cancer in its early stage is considered to be crucial in increasing the chances of successful treatment and decreasing the cancer death rate (2). Several diagnostic techniques are commonly used clinically, including blood chemistry tests (3), complete blood count (CBC) (4), cytogenetic analysis (5), immunophenotyping (6), liquid biopsy (7), cancer biomarker tests (8), imaging tests (9) etc. Collectively, these methods take advantage of cancer-associated molecular or phenotypical abnormalities and can be used in combinatory ways. Among the methods mentioned above, cancer biomarker testes are prominent in improving cancer patient management by enhancing diagnostic efficacy and accuracy (8). Cancer biomarkers refer to the measurable biochemical products that are produced by cancer cells or by body in response to the cancerous cells, such as proteins and nucleic acids (8, 10, 11). In monitoring these biomarkers, cancer type and risk can be determined and evaluated. Moreover, antibody-based cancer therapy is designed based on the presences and functions of these biomarkers.

Attributed to its high affinity and specificity, antibody-based cancer therapy has been recognized as one of the most powerful cancer therapeutics. In almost 30 years of its development, the global market of cancer antibody has grown exponentially (Table 1.) and is forecasted to be around US$80 billion by the end of 2026 (12). The therapeutic functionality of antibodies is achieved through the mechanisms of either the blockade of molecule-cell interactions or the modulation of human immune responses (12).

In blocking the molecule-cell interaction, monoclonal antibodies exert their functions through interfering the receptor-ligand interactions that are vital for tumor

survival and growth. For example, human epidermal growth factor receptor 2 (HER2) that control how cells grow and divide is the target of monoclonal antibodies like Herceptin, and by blocking HER2, the overgrowth of certain tumor cells can be downregulated (13). Similarly, monoclonal antibody bevacizumab prevents the binding of vascular endothelial growth factor (VEGF) to its receptors, VEGFR1 and VEGFR2, to inhibit the formation of new blood vessels and modulate the tumor-induced immunosuppression (14).

It also has been demonstrated that monoclonal antibodies can be used to modulate the immune activities through stimulatory or inhibitory pathways. The interactions between Fc region of the antibodies and activating Fcγ receptors on the immune cells can be utilized to eliminate cancer cells by antibody-dependent cellular cytotoxicity (ADCC) or/and antibody-dependent cellular phagocytosis (ADCP) (15). In ADCC, NK cells are well-studied to play a major role in tumor clearance. NK cells have the ability to express FcγRIIIA and/or FcγRIIC, which enable them to attach to the Fc region of immunoglobulins and convey activating signals internally. Upon activation through Fc receptors with antibodies attached to target cells, NK cells can eliminate target cancer cells through releasing the granules containing perforin and granzymes, it also releases cytokines such as interferon-γ to recruit adaptive immune cells (16). Macrophages with immense ability of phagocytosis, on the other hand, serve as critical immune effectors of therapeutic antibodies through the process of ADCP by expressing all classes of Fcγ receptors (17). Additionally, antibody-mediated antitumor effects also have been linked to complement-based mechanisms, which can act either directly via complement-dependent cytotoxicity (CDC) or indirectly through complement-dependent cellular cytotoxicity (CDCC) and complement-dependent cellular phagocytosis (CDCP) (18). Moreover, immune cells like T cells and NK cells also express inhibitory receptors which are used to downregulate immune activities to

maintain homeostasis (19). Cytotoxic T-lymphocyte-associated protein 4, or CTLA-4, a molecule that functions as an immune checkpoint, is expressed at high levels on cytotoxic T lymphocytes (20). Through its interaction with and high affinity for the B7 ligand, CTLA-4 promotes immunosuppression and enables tumors to evade immune surveillance. It competitively inhibits CD28 co-receptor interactions, resulting in the blockade of stimulatory signaling and the suppression of T cell activity (21). Similarly, programmed cell death protein 1 (PD-1) is another well-studied inhibitory receptor on T cells, and many tumors overexpress its ligand, PD-L1, to achieve immunoevasion (22). Many monoclonal antibodies are designed to block these inhibitory interactions between tumor cells and immune cells to sustain the immune activities, such as PD-1 inhibitors: Pembrolizumab (Keytruda) (23), Nivolumab (Opdivo) (24), and Cemiplimab (Libtayo) (25); PD-L1 inhibitors: Atezolizumab (Tecentriq) (26), Avelumab (Bavencio) (27), and Durvalumab (Imfinzi) (28); and CTLA-4 inhibitors: Ipilimumab (Yervoy) (29) and Tremelimumab (Imjuno) (30). This type of therapy was given the name of immunotherapy based on its idea of treating cancer by targeting immune cells instead of cancer cells (31).

Table 1. US or EU Approved Cancer Monoclonal Antibodies (12)

INN	Drug Name	Company	Target	Year of Approval
Rituximab	Rituxan	Genentech (Roche)	CD20	1997 (US) 1998 (EU)
Trastuzumab	Herceptin	Genentech (Roche)	HER2	1998 (US) 2000 (EU)
Alemtuzumab	Campath	Genzyme (Sanofi)	CD52	2001 (US) 2001 (EU)
Ibritumomab tiuxetan	Zevalin	Biogen, Acrotech	CD20	2002 (US) 2004 (EU)
Tositumomab-I131	Bexxar	Corixa (GSK)	CD20	2003 (US)
Cetuximab	Erbitux	ImClone (Eli Lilly)	EGFR	2004 (US) 2004 (EU)
Bevacizumab	Avastin	Genentech (Roche)	VEGF	2004 (US) 2005 (EU)
Panitumumab	Vectibix	Amgen	EGFR	2006 (US) 2007 (EU)
Catumaxomab	Removab	Fresenius, Trion Pharma	EpCAM/CD3	2009 (EU)
Ofatumumab	Arzerra	Genmab, Novartis	CD20	2009 (US) 2010 (EU)
Denosumab	Xgeva	Amgen	RANKL	2010 (US) 2011 (EU)
Ipilimumab	Yervoy	Medarex (BMS)	CTLA-4	2011 (US) 2011 (EU)
Pertuzumab	Perjeta	Genentech (Roche)	HER2	2012 (US) 2013 (EU)
Obinutuzumab	Gazyva	Genentech (Roche)	CD20	2013 (US) 2014 (EU)
Ramucirumab	Cyramza	Dyax, Eli Lilly	VEGFR2	2014 (US) 2015 (EU)
Nivolumab	Opdivo	Medarex (BMS)	PD-1	2014 (US) 2015 (EU)
Pembrolizumab	Keytruda	Merck & Co.	PD-1	2014 (US) 2015 (EU)
Blinatumomab	Blincyto	Micromet (Amgen)	CD19, CD3	2014 (US) 2015 (EU)
Necitumumab	Portrazza	ImClone (Eli Lilly)	EGFR	2015 (US) 2016 (EU)
Dinutuximab	Unituxin	United Therapeutics	GD2	2015 (US) 2017 (EU)
Daratumumab	Darzalex	Genmab, Janssen (J&J)	CD38	2015 (US) 2016 (EU)
Elotuzumab	Empliciti	Abbvie, BMS	SLAMF7	2015 (US) 2016 (EU)
Olaratumab	Lartruvo	ImClone (Eli Lilly)	PDGRFa	2016 (US) 2016 (EU)

Table 1. (Continued)

INN	Drug Name	Company	Target	Year of Approval
Atezolizumab	Tecentriq	Genentech (Roche)	PD-L1	2016 (US) 2017 (EU)
Avelumab	Bavencio	EMD Serono, Pfizer	PD-L1	2017 (US) 2017 (EU)
Durvalumab	Imfinzi	MedImmune (AstraZeneca)	PD-L1	2017 (US) 2018 (EU)
Mogamulizumab	Poteligeo	Kyowa Kirin	CCR4	2018 (US) 2019 (EU)
Cemiplimab	Libtayo	Regeneron, Sanofi	PD-1	2018 (US) 2019 (EU)
Moxetumomab pasudotox	Lumoxiti	Innate Pharma, AstraZeneca	CD22	2018 (US) 2021 (EU)
Isatuximab	Sarclissa	ImmunoGen, Sanofi	CD38	2020 (US) 2020 (EU)
Tafasitamab	Monjuvi, Minjuvi	MorphoSys, Incyte	CD19	2020 (US) 2021 (EU)
Naxitamab	Danyelza	Y-mAbs	GD2	2020 (US)
Dostarlimab	Jemperli	GSK	PD-1	2021 (US) 2021 (EU)
Amivantamab	Rybrevant	Genmab, Janssen (J&J)	EGFR, cMET	2021 (US) 2022 (EU)
Tebentafusp	Kimmtrak	Immunocore	Gp100, CD3	2022 (US)
Teclistamab	TECVAYLI	Jannsen (J & J)	CD3, BCMA;	2022 (US) 2022 (EU)
Tremelimumab	Imjudo	MedImmune (AstraZeneca)	CTLA-4	2022 (US)
Monetsuzumab	Lunsumio	Genentech (Roche)	CD20, CD3	2022 (EU)

2. Cancer-Associated Glycans

In recent decades, cell surface glycans have been unveiled to play essential roles in many biological processes, both normal and pathological (32, 33). The understanding of these processes potentiates numerous clinical practices, from blood transfusion (34) to inflammation attenuation (35), and, in foreseeable future, cancer immunotherapy (36~39). However, investigating glycans is usually perceived as a daunting task since they are among the most structurally and functionally diverse biomolecules in living systems, which is mostly owing to the variety of both monosaccharide building blocks and glycosidic linkages (32). Also, given the fact that glycans are found attached to proteins, lipids, and, most recently discovered, RNAs (40), glycoconjugates are believed to be possessing even more extensive diversity. Accordingly, till today, our basic knowledge of fundamental glycobiology is still limited, which impedes the development of glycan-based or glycan-targeted therapies.

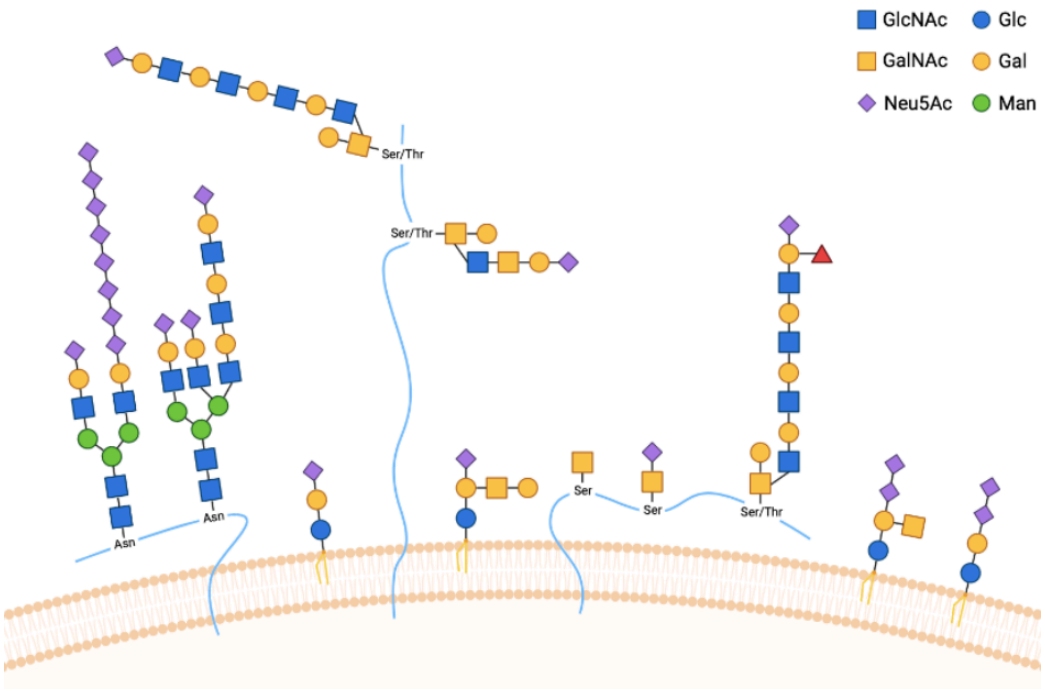

Figure 1. Cancer-associated glycan structures. Created with BioRender.com.

In cancer, drastic alteration of glycosylation patterns has been identified for decades, including increased sialylation, increased branched N-glycan structures, and truncated O-glycan structures, and have been demonstrated to be correlated with many pathological events in cancer progression including proliferation, migration, tissue invasion, and apoptotic evasion (Figure 1.)(39, 41~44). These distinguishable altered patterns are proven to be able to potentiate the development of novel cancer diagnostics and therapeutics (45). One of the most prominent examples is the increased sialylation, or hypersialylation. With abundant glycans terminated with sialic acids, cancer cells forge a signature of healthy cells that silences immune surveillance by recruiting inhibitory receptors like sialic acid-binding immunoglobulin-like lectins (Siglecs) on lymphocytes (46~50). Siglecs-7 or -9 on NK cells, for example, has several cytosolic immunoreceptor tyrosine-based inhibitory motifs (ITIMs) that can suppress the activation signals from the NK cells-activating receptors, such as FcγRIII and NKG2D,

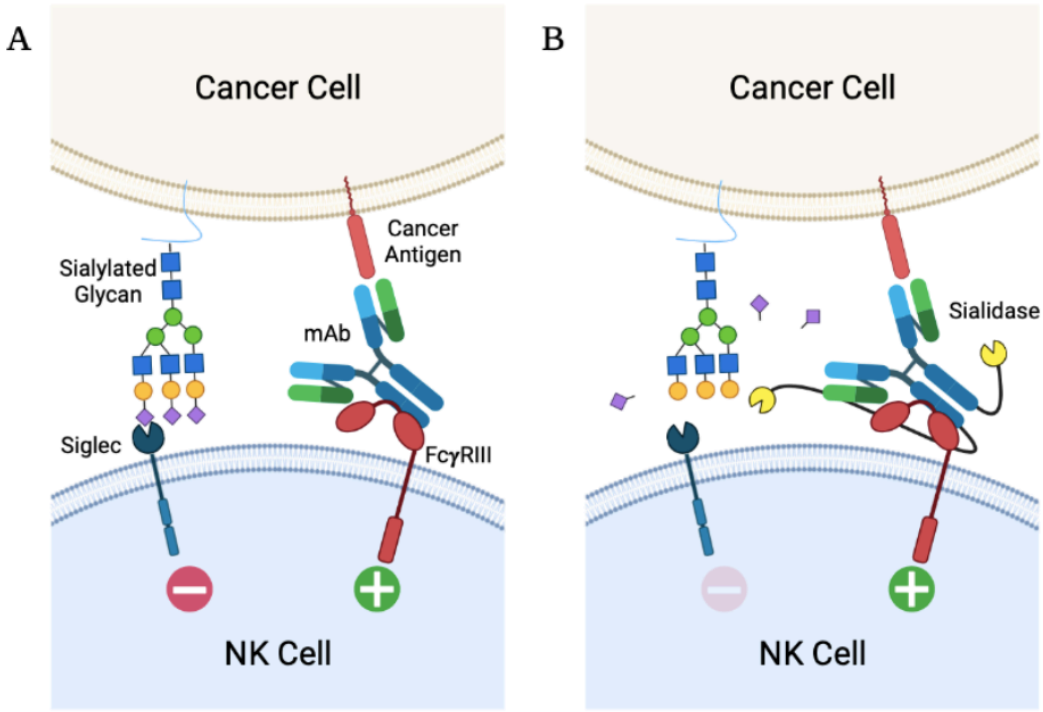

Figure 2. Enhancement strategy of cancer-cell eliminating ability through glycocalyx editing. (A) Hypersialylation leads to NK-cell inhibition. (B) Antibody-sialidase conjugate reduces the cancer immunoevasion. Created with BioRender.com.

when binding to the overexpressed sialic acids in cancer cells (51). Based on this finding, Carolyn Bertozzi's lab developed a glycocalyx editing technique where sialidases were linked to HER2-targeting therapeutic monoclonal antibody Trastuzumab, and the treatment with this kind of antibody-sialidase conjugate has been proven to be able to promote the HER2(one-+)-cancer cell elimination (Figure 2.)(52). Another recognizable cancer-associated glycosylation signature would be the overexpression of bulky glycoproteins, such as MUC1 which is a kind of heavily glycosylated transmembrane protein that can be found on the surface of many healthy epithelial cells including those of the respiratory, gastrointestinal, and reproductive tracts, as well as many cancer cells (41, 43~45) (Figure 3.). And these bulky glycoproteins have been shown to be able to promote tumor cell growth and survival, as well as to enhance metastasis through facilitating of integrin clustering, adhesion and signaling, which is resulted from the mechanical forces imposed by these bulky glycoproteins (44).

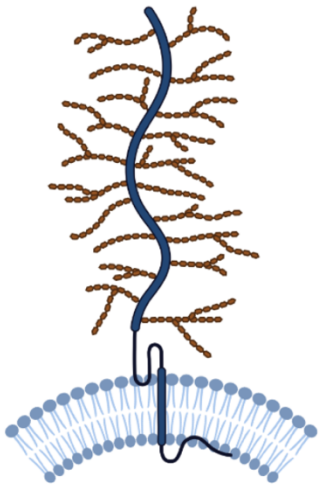

Figure 3. Cartoon of bulky glycoprotein MUC1 with the extracellular domain, transmembrane domain, and cytosolic domain showing (from top to bottom). Created with BioRender.com.

3. Strategies for Glycan Study

A better understanding towards cancer glycobiology could potentially facilitate the development of faster and more accurate cancer diagnostic techniques, as well as future cancer therapies. One traditional glycans identification and quantification method is using mass spectrometry, which majorly suffered from the disadvantages including time-consuming process, expensive equipment, and detachment from biological environment (53, 54). About 20 years ago, Carolyn Bertozzi's lab developed an in situ and in vivo glycan imaging method that took advantage of metabolic labeling and bioorthogonal chemistry (55~60), in which one monosaccharide subunit was replaced by its artificial analog with a bioorthogonal functional group. Although this method has opened a new avenue for cell-surface glycan imaging, it is not without limitations. To begin with, the glycan revelation is constrained to monosaccharide level—the basic building block of glycans, and no structural information can be provided. Moreover, even though those monosaccharide analogs were incorporable in the natural metabolic pathways, the concern of uncertainty of their effects on glycan-expression level, glycan-biosynthesis authenticity, and cell stress response still remains. Alternatively, glycan-binding proteins (GBPs) as powerful tools are widely accepted and utilized by chemical and biological research community and give rise to a growing research area of GBPs engineering to fulfill the increasingly comprehensive clinical demands (53), especially those in cancer diagnoses and therapies.

GBPs can be subcategorized into three groups: lectins, carbohydrate-binding module s (CBMs), and adaptive immune proteins. CBMs (Carbohydrate-Binding Modules) were firstly recognized as a binding domain that link to glycoside hydrolases and glycotransferases, that binds to the glycan substrates to its increase local concentration which consequently improving the catalytic efficiency of the enzyme (61). For example, *Ruminococcus gnavus*, a significant member of the gut microbiota

of the healthy human gut, expresses an intramolecular trans-sialidase (IT-sialidase) that contributing to the adaptation of gut bacteria to the mucosal environment by providing 2,7-anhydro-sialic acid as a preferential source of nutrients, and this IT-sialidase comprises a catalytic glycoside hydrolase domain, RgGH33, and a carbohydrate binding module, RgCBM40 (62). CBMs are organized into 73 families on the basis of their amino acid sequence similarity, most interact with plant cell wall glycans, but five CBM families have been categorized as mammalian glycan-binding domains: CBM32, CBM40, CBM47, CBM51 and CBM57 (63). Within these, the members of CBM40 are known to bind to Neu5Ac, which was first verified with the CBM located at the N-terminus of GH33 (glycoside hydrolase 33) sialidase from *Vibrio cholerae* (64). A member of the CBM40 family, *Clostridium perfringens*-NanI-CBM40 (CpCBM40_NanI), has been characterized with the highest affinity value for α(2,3)-sialyl-lactose (Kd ~30 μM) in this class of protein (63), this indicated that CpCBM40_NanI would be an exceptional candidate for the cell-surface imaging of glycans that are rich in the N-acetylneuraminic acid (Neu5Ac), the most common form of sialic acid on mammalian cells. As shown in supplementary figure 1, the 3D structure of CpCBM40_NanI consists of one alpha helix and one beta sandwich of two anti-parallel beta sheets. To further improve the binding affinity, we propose to fuse two CBM40 together which will render avidity to this module inspired by nature's multivalency approach to gaining increased binding affinity (65). Moreover, an efficient site-specific protein modification method will also be crucial in rendering additional function to glycan-binding proteins, such as fluorophore conjugation. And by genetically engineering a versatile polypeptide handle to diCBM40, diCBM40-LPETG will be acquired a powerful ability to be chemically modified by sortase-mediate transpeptidation (66).

Sortase was first discovered as a surface enzyme in *Staphylococcus aureus* that anchors other surface proteins to cell wall (67). During this process of cell-wall anchoring, sortase will recognize a sorting signal with LPXTG motif followed by a stretch of 15-22 hydrophobic amino acid residues and a tail of 5-12 mostly charged residues at the C-terminal of target protein, and then this target protein will be cleaved between the threonine and glycine residues within the LPXTG motif. The carboxyl group of threonine residue will be consequently anchored to the cysteine residue of sortase through a thioester bond followed by a nucleophilic attack from a nearby amino group of pentaglycine crossbridges, normally lipid II, a membrane-anchored precursor of cell-wall synthesis, this surfaced-tethered lipid II may subsequently be incorporated into the peptidoglycan (Figure 4.)(68~73).

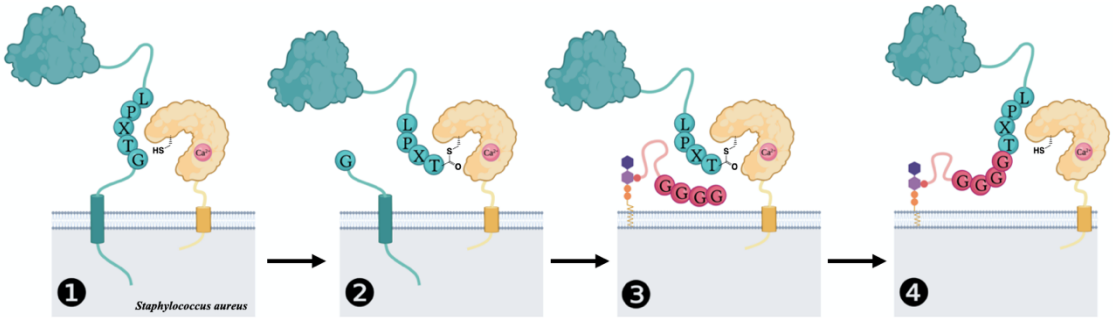

Figure 4. Sortase-mediated transpeptidation found on the surface of *Staphylococcus aureus*. ❶ Sortase recognition of LPXTG motif on target proteins. ❷ Nucleophilic substitution reaction with cysteine residue in sortase active site. ❸ and ❹ Target protein undergoes transpeptidation to the oligoglycine peptide on lipid A. Created with BioRender.com.

Upon understanding of this natural cell-wall synthesis pathway, scientists have been successfully utilizing the same mechanism to perform in vitro protein-peptide and protein-protein ligation (74), polystyrene beads modification with eGFP (75), cell-surface protein labeling (76) and antibody labeling (77). Essentially, as long as the target protein is engineered to obtain a LPXTG motif, it can be labeled with a probe that

contains an oligoglycine chain with a free amino group (73). With the advance in protein characterization methods, more insights have been brought into the active sites, structures, and kinetics of different kinds of sortase. The first thing for researchers to notice was that the thiol group of cysteine-184 (C184) plays an essential role in sortase activity as a nucleophile to cleave the peptide bond between threonine and glycine residues, and mutation of cysteine-184 to alanine abolishes sortase activity in vitro and in vivo (78). Later study hypothesized that N98, H120, and C184 may form a catalytic triad that mediates the transpeptidation reaction and are positioned within a large hydrophobic pocket suitable for sorting signal binding derived by analogy with the papain/cathepsin protease family (79).Since sortase itself is also a kind of membrane-anchored enzymes with class A sortases adopt a type II membrane topology (N terminus inside, C terminus outside the cytoplasm) and class B a type I (N terminus outside, C terminus inside the cytoplasm), scientists proposed that truncation of the membrane anchor segment will not affect the enzymatic activity and increase the solubility at the same time, which made sortase more adaptable in various scenarios (72, 80). Sortase A can be further truncated, denoted as $SrtA_{\Delta N59}$, to contain only the presumed catalytic core of sortase (residues 60-206) (79). In-depth structural study with NMR spectroscopy revealed that $SrtA_{\Delta N59}$ possesses an unseen eight-stranded β-barrel fold that includes two short helices and several loops (79). It has also been shown that the enzymatic activity of sortase A is stimulated by Ca^{2+}, both in wide type sortase A (WT SrtA) and $SrtA_{\Delta N59}$, via allosteric activation mechanism where the binding of Ca^{2+} stabilizes the closed conformation of enzyme-substrate complex (79, 80), and that mutations of both Glu105 and Glu108 resulted in Ca^{2+}-independent activity without affecting its substrate specificity (81) Scientists then sought to improve the catalytic activity of sortases to make this tool more efficient. David Liu's lab successfully developed an evolved sortase A by using yeast display, a directed evolution platform, where the P94R, D160N,

D165A, K190E, K196T pentamutant $SrtA_{\Delta N59}$ (e5M SrtA) (Figure 4.) has a 120-fold higher k_{cat}/K_M LPETG and a 20-fold higher K_M GGG, compared with WT SrtA (82).

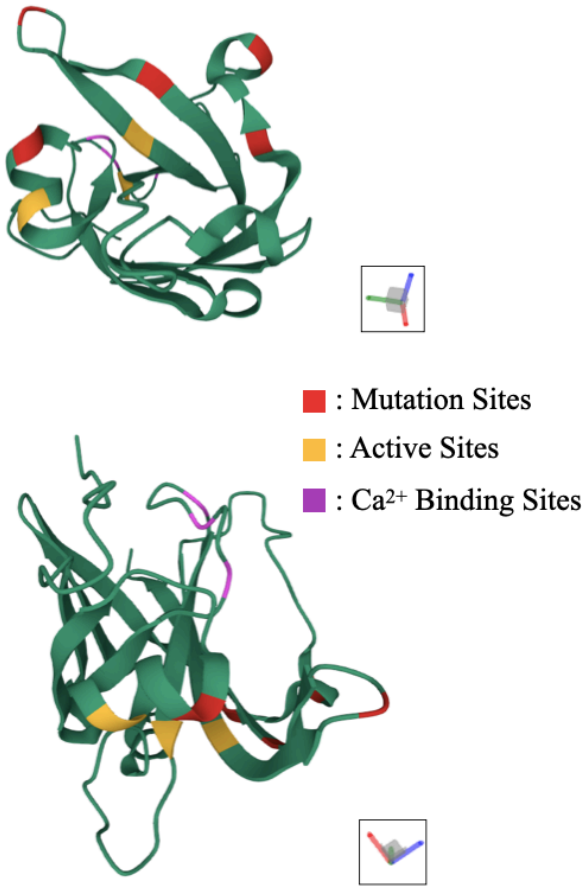

Figure 5. Evolved sortase A 3D-structure with the mutation sites, active sites and calcium ion binding sites highlighted. PDB: 1T2P.

Single-chain variable fragment (scFv) antibodies are also perceived as one of the emerging candidates in cancer diagnostic and therapeutic application, owning to their smaller sizes and properties of being easily engineered while retaining the similar targeting affinity and specificity as their counterpart antibodies (83~85). scFv usually comprises a light chain, V_L, and a heavy chain, V_H, that are tethered with each other through a flexible linker that usually contain many glycine units for its flexibility and some serine units for its solubility (86), and there are two orientations of this connection,

either N terminus of V_H connected with C terminus of V_L (V_LV_H) or vis versa (V_HV_L), in which binding affinities and expression levels can be differed (83, 87). In glycan study, it is promising to harness the great specificity, affinity, and reconstruction convenience scFv antibodies offered and include them into the molecular toolkit for cell-surface glycans targeting and imaging. Several different scFv candidates can be considered, including scFv-BR96 and scFv-Unituxin. BR96 binds specifically to LeY tetra-saccharide, a carbohydrate antigen was found to be expressed on a range of tumors including, lung carcinoma, lung adenocarcinoma, ovarian carcinoma, and colorectal adenocarcinoma (88). Studies has shown that BR96 can inhibit tumor cell growth, and when bound to adherent cells, is internalized via coated pits to multivesicular bodies, and finally, degraded in lysosomes (89). Unituxin, or Dinutuximab, is a chimeric monoclonal antibody targeted against the disialoganglioside GD2 that is highly over-expressed in neuroblastoma cells (90~92). Neuroblastoma is a cancer that develops from immature nerve cells found in several areas of the body (91, 93). One key player in the anti-tumor response of Dinutuximab is NK cells. These cells are capable of killing antibody-bound NB cells via ADCC (92). Another type of GBPs—Siglec-like binding regions (SLBRs)—that were firstly discovered in Streptococci, part of human normal oral microbiota, can be also considered (94). These organisms express serine-rich adhesins containing Neu5Ac(α2-3)Gal-recognizing SLBRs on their cell surfaces (95). The same engineering and modification methods can be also applied to these classes of glycan-binding protein for the purpose of developing cell surface glycan imaging molecular toolkit.

II. Methods

1. Glycan-Binding Protein Engineering, Expression, Purification and Modification

eSrtA Expression. pET29-e5M SrtA-His transformed E. coli BL21(DE3) were cultured in at 37 °C in LB with 100 μg/mL kanamycin until OD600 = 0.5~0.7. For Induction, IPTG was added to the final concentration of 0.5 mM, cell cultures then induced for 16hr 25℃ shaker. For protease inhibitor, Pierce Protease Inhibitor Tablets (working concentration: 1 tablet/50ml solution) were used or not used in BugBuster Master Mix lysis buffer. After induction, cell cultures were then pelleted down with 2000 g for 10 min at 4°C, cell pellets were resuspended by BugBuster Master Mix lysis buffer with or without Pierce Protease Inhibitor followed by incubation on rotator at 4°C for 30min. Cell lysates were centrifuged with 30000 g for 20 min at 4°C, supernatant and precipitation were then separated for later analysis. Protein analysis was performed by SDS-PAGE followed by Western-Blot and Coomassie blue staining.

eSrtA Purification. E. coli BL21(DE3) transformed with pET29-e5M SrtA-His expression plasmids were cultured at 37 °C in LB with 50 μg/mL kanamycin until OD600 = 0.6. IPTG was added to a final concentration of 0.5 mM and protein expression was induced for 16 hours at 25 °C. The cells were harvested by centrifugation and resuspended in lysis buffer (50 mM Tris-HCl pH 7.5, 150 mM NaCl supplemented with 5 mM MgCl2, 10 mM imidazole and 10% v./v. glycerol). Cells were lysed by sonication and the clarified supernatant was purified on Ni-NTA agarose following the manufacturer's instructions. Fractions from column were collected, as judged by Bradford assay, and then were consolidated and dialyzed against tris-buffer saline (50 mM Tris-HCl pH7.5, 150 mM NaCl). Non-induced, induced, lysate precipitation, lysate supernatant, flow through, elutes, and final product were analyzed with Western Blot and Coomassie blue staining.

diCBM40-0, 1.1, and 3.0 Construction. One forward primer and one reverse primer were used for the construction of diCBM40-0:
5'-GCTGCTAGCATGTTATCATCATTAGGTGAGTAC-3', and
5'-CTGACTCGAGTTTGGTTTCACCGGTTTTGC-3'; one forward primer and two reverse primers were used for the construction of diCBM40-1.1:
5'- GCTGCTAGCATGTTATCATCATTAGGTGAGTAC-3',
5'- CGGGAGGGAGCCACCACCTTTGGTTTCACCGGTTTTGC-3', and
5'- ATTTCTCGAGACCTGTTTCCGGGAGGGAGCCACCACCTT-3'; one forward primer and two reverse primers were used for the construction of diCBM40-3.0:
5'- GCTGCTAGCATGTTATCATCATTAGGTGAG-3',
5'- CTCACTCCCATTGAGAGCTTTGGTTTCACCGGTTTTG-3',
5'- CCCACTGCCGGATCCTAACTCACTCCCATTGAGAGCTTT-3',and
5'-GGACTCGAGACCTGTTTCTGGTAGCCCACTGCCGGATCCTAAC-3'. They were designed as to include the NheI/XhoI restriction sites. For these primer design, they were considered to include the following properties: 1) having G/C content of 40~60%; 2) starting and ending with 1-2 G/C pairs; 3) having melting temperature of 50~60℃; 4) each annealing pair should have a Tm difference within 5℃; 5) primers should not be having complementary region within their Figure 6. In gel fluorescence assay of protein conjugation reaction result. sequences: 6) if a restriction site is included at the 5' end of your primer, a 3-6 base pair "clamp" should be added upstream in order for the enzyme to cleave efficiently. The PCR products after two-round PCR and pET21a plasmid vector were digested with restriction enzymes, NheI and XhoI (Supporting Figure 2.), and ligated by T4 ligase, the final products were transformed to E. coli DH5α and stored under -80℃ for future usage.

diCBM40 Expression. pET21a-diCBM40-(LPETG) transformed E. coli BL21(DE3) were cultured in at 37 °C in LB with 100 μg/mL ampicillin until OD600 =

0.5~0.7. The testing condition include with or without 42℃ heat shock for 20min before adding IPTG; with or without proteases inhibitor in lysis solution; 16℃, 30℃, and 37℃ for induction. For induction, IPTG was added to the final concentration of 0.5 mM, cell cultures then induced for 20hr in 16℃, 30℃, and 37℃ shakers. For protease inhibitor, Pierce Protease Inhibitor Tablets (working concentration: 1 tablet/50ml solution) were used or not used in BugBuster Master Mix lysis buffer. After induction, cell cultures were then pelleted down with 2000 g for 10 min at 4°C, cell pellets were resuspended by BugBuster Master Mix lysis buffer with or without Pierce Protease Inhibitor followed by incubation on rotator at 4°C for 30min. Cell lysates were centrifuged with 30000 g for 20 min at 4°C, supernatant and precipitation were then separated for later analysis. Protein analysis was performed by SDS-PAGE followed by Western-Blot and Coomassie blue staining.

diCBM40 Purification. E. coli BL21(DE3) transformed with pET21a-diCBM40-(LPETG) expression plasmids were cultured at 37 °C in LB with 50 μg/mL kanamycin until OD600 = 0.6. IPTG was added to a final concentration of 0.5 mM and protein expression was induced for 16 hours at 25 °C. The cells were harvested by centrifugation and resuspended in lysis buffer (50 mM Tris-HCl pH 7.5, 150 mM NaCl supplemented with 5 mM MgCl2, 10 mM imidazole and 10% v./v. glycerol). Cells were lysed by sonication and the clarified supernatant was purified on Ni-NTA agarose following the manufacturer's instructions. Fractions from column were collected, as judged by Bradford assay, and then were consolidated and dialyzed against tris-buffer saline (50 mM Tris-HCl pH7.5, 150 mM NaCl). Non-induced, induced, lysate precipitation, lysate supernatant, flow through, elutes, and final product were analyzed with Western Blot and Coomassie blue staining.

scFv Expression. pET28a-scFv-(LPETG) transformed E. coli SHuffle were cultured in at 30 °C in LB with 50 μg/mL kanamycin until OD600 = ~0.6. The testing

condition include: 16℃, and 30℃ for induction temperature; 0.05mM/0.5mM/1mM for IPTG concentration; 16hr/48hr for induction time. After induction, cell cultures were then pelleted down with 2000 g for 10 min at 4°C, cell pellets were resuspended by BugBuster Master Mix lysis buffer with or without Pierce Protease Inhibitor followed by incubation on rotator at 4°C for 30min. Cell lysates were centrifuged with 30000 g for 20 min at 4°C, supernatant and precipitation were then separated Supplementary Figure 1. Sortase-Mediated Cell Surface Peptide Anchoring Mechanism. Figure 5. DMSO Tolerance Test of scFv-Unituxin-LPETG (A), SLBR-N-LPETG (B), and scFv-BR96-LPETG (C) for later analysis. Protein analysis was performed by SDS-PAGE followed by Western-Blot and Coomassie blue staining.

scFv Purification. E. coli SHuffle transformed with pET28a-scFv-(LPETG) expression plasmids were cultured at 30 °C in LB with 50 μg/mL kanamycin until OD600 = 0.6. IPTG was added to a final concentration of 0.05 mM and protein expression was induced for 48 hours at 16 °C. The cells were harvested by centrifugation and resuspended in lysis buffer (50 mM Tris-HCl pH 7.5, 150 mM NaCl supplemented with 10 mM imidazole and 10% v./v. glycerol). Cells were lysed by homogenizer and the clarified supernatant was purified on Ni-NTA agarose following the manufacturer's instructions. Fractions from column were collected, as judged by Bradford assay, and then were consolidated and dialyzed against tris-buffer saline (50 mM Tris-HCl pH7.5, 150 mM NaCl). Non-induced, induced, lysate precipitation, lysate supernatant, flow through, elutes, and final product were analyzed with Western Blot and Coomassie blue staining.

Protein Concentration Measurement with Bradford Assay. Pilot test the protein samples concentration by comparing the color intensities of protein samples with pre-made BSA500 and dilute the protein sample further into proper concentration if necessary(within the range of protein standard used to make the assay accurate).

Setting two parallel testing rows with the standard BSA gradient, add 2ul protein sample and 100ul 1xBradford Assay Dye to each well, and measure the 595nm absorption with plate reader. Calculate the protein concentration by fitting the protein sample absorption to the standard BSA absorption regression line.

e5M SrtA-mediated Protein Conjugation with Oligoglycine Dye. Mix a solution containing 10–50 μM target protein (diCBM40-LPETG, scFv-LPETG), 20–150 μM sortase and 1–2 mM oligoglycine probe in 1× sortase buffer (500 mM Tris-HCl pH 7.5, 1.5 M NaCl supplemented with 100 mM CaCl2). The controls to be included are as follows: target protein only, sortase only, oligoglycine probe only, target protein and sortase, target protein and oligoglycine probe, sortase and oligoglycine probe. Incubate the reactions at RT or at 37 °C. Take 1-μl aliquots after 2, 4, 6, 8 and 16 h. Add 1× LDS gel-loading buffer to the aliquots to stop the reaction and boil it for 2 min. Analyze the aliquots by SDS-PAGE followed by Western Blot and Coomassie blue staining.

2. Mammalian Cell Lines Culture

Mammalian Cell MCF10A and MCF10A GNE KO Culture. Using media of DMEM/F12 for mammalian cell culture, which contains 5% horse serum (HS), 1x Penicillin-Streptomycin (PS), 20ng/ml EGF (Epidermal Growth Factor), 0.5ug/ml hydrocortisone, 100ng/ml Cholera toxin, and 10ug/ml insulin. Thaw the cell stock from liquid nitrogen tank in 37℃ water bath to slushy condition. Resuspend and dilute the cell with pre-warmed up DMEM/F12 media and transfer the cell culture into 15ml centrifuge tube, and then pellet down the cell with 1200rpm for 5min. Discard the supernatant and resuspend the cell with DMEM/F12 media. Then dilute the cell culture to $1x10^4$ cell/ml, and transfer into tissue flask, and culture the cell in 37℃ 5% CO_2 incubator for 48hr.

Mammalian Cell SKOV3, SW2, and A549 Culture. Using media of DMEM for mammalian cell culture, which contains 5% Fetal Bovine Serum (FBS), 1x Penicillin-Streptomycin (PS). Thaw the cell stock from liquid nitrogen tank in 37°C water bath to slushy condition. Resuspend and dilute the cell with pre-warmed up DMEM media and transfer the cell culture into 15ml centrifuge tube, and then pellet down the cell with 1200rpm for 5min. Discard the supernatant and resuspend the cell with DMEM media. Then dilute the cell culture to $1x10^4$ cell/ml, and transfer into tissue flask, and culture the cell in 37°C 5% CO_2 incubator for 48hr.

Mammalian Cell SH-SY5Y Culture. Using media of DMEM/F12 for mammalian cell culture, which contains 10% Fetal Bovine Serum (FBS), 1x Penicillin-Streptomycin (PS). Thaw the cell stock from liquid nitrogen tank in 37°C water bath to slushy condition. Resuspend and dilute the cell with pre-warmed up DMEM media and transfer the cell culture into 15ml centrifuge tube, and then pellet down the cell with 1200rpm for 5min. Discard the supernatant and resuspend the cell with DMEM/F12 media. Then dilute the cell culture to $1x10^5$ cell/ml, and transfer into tissue flask, and culture the cell in 37°C 5% CO_2 incubator for 4~7days.

3. Cell-Surface Antigens Binding Assay

Glycan ELISA. Prepare 4ug/ml BSA and GD2-BSA with PBS. 1/4 of the plate will be just (50ul/well, 4ug/ml)BSA, 1/4 will be (50ul/well, 4ug/ml) GD2-BSA, 1/2 of the plate will be blanked with PBS. Coat the plate, make sure the surface is completely covered, incubate the plate with lid in 4℃ overnight. Making blocking solution: 5% w./v. milk in PBS, collect the cell plate from 4℃ fridge, discard the blocking solution into sink by flicking and taping on the paper towel. Wash the plate well 1~3 times with 100ul PBS, for each wash tapping the plate followed by flicking and taping on paper towel. Add pre-made 200ul blocking solution to the plate, blocking incubate the plate

with lid in 4℃ overnight or room temperature shacking for 2 hours. Making 4uM scFv-Unituxin solution in 2.5% w./v. milk in PBST, add 150ul to each well in the row A; adding 120ul 2.5% w./v. milk in PBST to all the rest of wells (row B to row H); take 40ul solution in the previous row to the next row for a 1:4 serial dilution. Collect the cell plate from 4℃ fridge or the shaker, discard the blocking protein solution into sink by flicking and taping on the paper towel; Wash the plate well 1 time with 150ul PBST, tapping the plate followed by flicking and taping on paper towels. Add 100ul binding protein from the no-binding plate into the corresponding wells of the binding plate; incubate the plate with lid in room temperature shacking for 1 hour. Secondary antibody solution making: 10ml 0.2 ug/ml (1/5000) aHis-HRP(ab1187) with 2.5% milk/PBST solution. Discard the binding protein solution into sink by flicking and taping on the paper towel. Wash the plate well 3 times with 150ul PBST, for each wash shaking tapping the plate followed by flicking and taping on paper towels. Add 100ul secondary antibody solution to His-tagged protein well(Unituxin), shaking incubate at room temperature on plate shaker for 1hr. Discard the secondary antibody solution into sink by flicking and taping on the paper towel. Wash the plate well 4 times with 150ul PBST, for each wash tapping the plate followed by flicking and taping on paper towels. Add 100ul HRP substrate—TMB into each well (prepare 10ml in reservoir). Waite until the color changing stops (can store the plate in a dark room while waiting), then add 100ul 2M H_2SO_4 into each well to stop the reaction; if color changes within 5min wait for maximum additional 10min, if not, waiting time should not exceed 30 min. Send to the plate reader for 450nm absorption measurement.

Cell Surface ELISA Assay. Cell in culture flask collected from 37℃ 5%CO_2 incubator, check cell health via observing the cell morphology by optical microscope. Discard the old DMEM media and wash the cell culture with 1x PBS to wash out old DMEM. Detaching the cell from the flask by adding 0.05% trypsin and incubate for

15min in 37℃ 5%CO_2 incubator, check the detachment by optical microscope. Add new DMEM to the culture flask to stop the trypsin digestion and transfer into centrifuge tube to pellet down the cell with 1200rpm for 5min. Discard the supernatant and resuspend the cell with DMEM. Using hemacytometer and 10ul cell culture for cell number counting and dilute the cell culture to 5x10^4 cell/ml, add 100ul to each well in 96-well culture plate, culture the cell in 37℃ 5% CO2 incubator for 24hr, after which discard the old DMEM:F12 media and add 100ul new media with 1ug/ml doxycycline for protein induction. Incubate the plate in 37℃, 5%CO2 incubator for another 24hr. For fixing and blocking the plate, discard the old DMEM with multichannel and wash each well with 150ul 1x PBS. Add 100ul fixation solution (4% (g/ml) PFA in 1xPBS) to each well, incubate at room temperature for 15min. Discard the fixation solution with multichannel and wash each well with 150ul PBS for 3 times. Add 150ul blocking solution (5% (g/ml) milk powder in 1xPBST) to each well, and seal the plate with sealing tape, followed by blocking at 4℃ overnight. After blocking, wash the plate well 3 times with 150ul PBST, and then add 100ul binding protein solution to each well in 2.5% w./v. milk in PBST, shaking incubate at room temperature on plate shaker for 1.5hr. Discard the binding protein solution and wash the plate well 3 times with 150ul PBST. Add 100ul secondary antibody solution (0.2 ug/ml (1/5000) aHis-HRP(ab1187); 1 ug/ml (1/2000) Avidin-HRP(Sigma E2886)) to each well, shaking incubate at room temperature on plate shaker for 1.5hr. Discard the secondary antibody solution and wash the plate well 3 times with 150ul PBST, and add 100ul HRP substrate—tetramethylbenzidine (TMB) into each well. Waite until the color changing stops (store the plate in a dark room while waiting), then add 100ul 2M H2SO4 into each well to stop the reaction. Lastly, send the plate to the plate reader for 450nm absorption measurement.

Fluorescence-activated cell sorting (FACS). Harvest the cell from culture step and adjust cell number to a concentration of 1x10^6 cell/ml in 1ml ice cold pre-made FACS buffer (0.1% BSA in PBS (W./V.)), and aliquot the cell into the Eppendorf tubes (250ul each). Add 0.1~10 ug/ml of primary antibody (scFv735; scFv-Unituxin) into corresponding tubes; dilution, if necessary, should be made in FACS buffer. Rotating incubate the cell samples for 1hr at 4℃, or room temperature for 30min. Wash the cells 2~3 times by centrifugation at 1500 rpm for 5 minutes and resuspend them 1ml of ice cold FACS buffer. Add conjugated secondary antibody(anti-His FITC, ab1206, Abcam; anti-Mouse AF488, A-11013, Thermo Fisher) 1ug to every 100ul cell sample (2.5ug per 250ul cell sample), resuspend the solution and rotating incubate the cell for 30min at 4℃ in the dark, or room temperature for 30min in the dark (wrapped with aluminum foil). Wash the cells 2~3 times by centrifugation at 1500 rpm for 5 minutes and resuspend them in 1ml of ice cold FACS buffer. Keep the cells in the dark on ice or at 4°C in a fridge until the scheduled time for FACS analysis. Data analysis was performed with FlowJo and FCS Express 7 Research.

4. Cell Imaging

Dilute the cell culture (MCF10A) to 1x10^4 cell/ml, add 2ml to glass-bottom 35mm dishes for each cell line, and culture the cell in 37℃ 5% CO_2 incubator for 48hr. Wash the dishes with 1ml 0.5%BSA PBS buffer 3 times, add 100ul the labeling protein solution into the glass center well and incubate the cell in dark ice-bath for 1hr. Wash the dishes with 1ml 0.5%BSA PBS buffer 3 times, add 1ml fresh 0.5% BSA PBS buffer to dishes and send them to imagining room; using 488(fluorophore) and 457(DAPI) channel for signal detecting.

III. Results and Discussions

1. Glycan-Binding Protein Engineering and Modification

We designed 4 different constructs for diCBM40 (Figure 6.), among which construct 1.1 and 3.0 will be at the most suitable for eSrtA-mediated protein conjugation. Compared the construct 0, constructs of 1.1, 2.0, and 3.0 contain a LPETG motif that can be recognized by sortase, and according to the transpeptidation mechanism the C-terminus His tag will be cleaved off upon completion of the reaction (73), which further facilitates the separation of protein conjugates and unreacted proteins. We then successfully expressed and purified the construct 0, 1.1, and 3.0 in E.

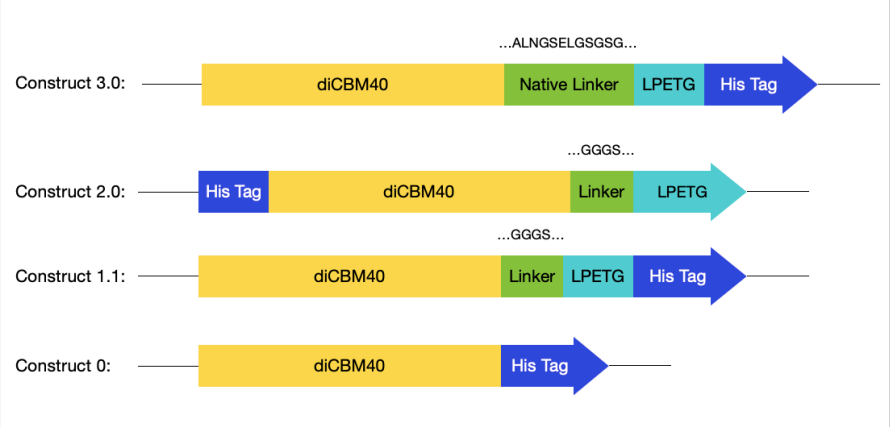

Figure 6. Systematic Design of diCBM40 Construct. Different positioning of His tags and LPETG tags are shown, the linker sequences are designed to be at least interfering the structural integrity.

Coli strain BL21(DE3) (Figure 7.). Construct diCBM40-0, 1.1, and 3.0 have molecular weight of 45.4kDa, 46.1kDa, and 46.9kDa, respectively, and the band shifting patterns in figure 2 can roughly demonstrate these size difference. Upon Ni-NTA resin purification, the unrelated protein was significantly reduced. Using BCA protein assay, the concentration of these constructs was measured. We then used the purified construct 0, 1.1, and 3.0 as the target protein in eSrtA-mediated protein conjugation reaction, in which we used AZDye647-GGG (Click Chemistry Tool) for probing the conjugated protein. After overnight conjugation reaction, diCBM40-1.1 and diCBM40-3.0 were

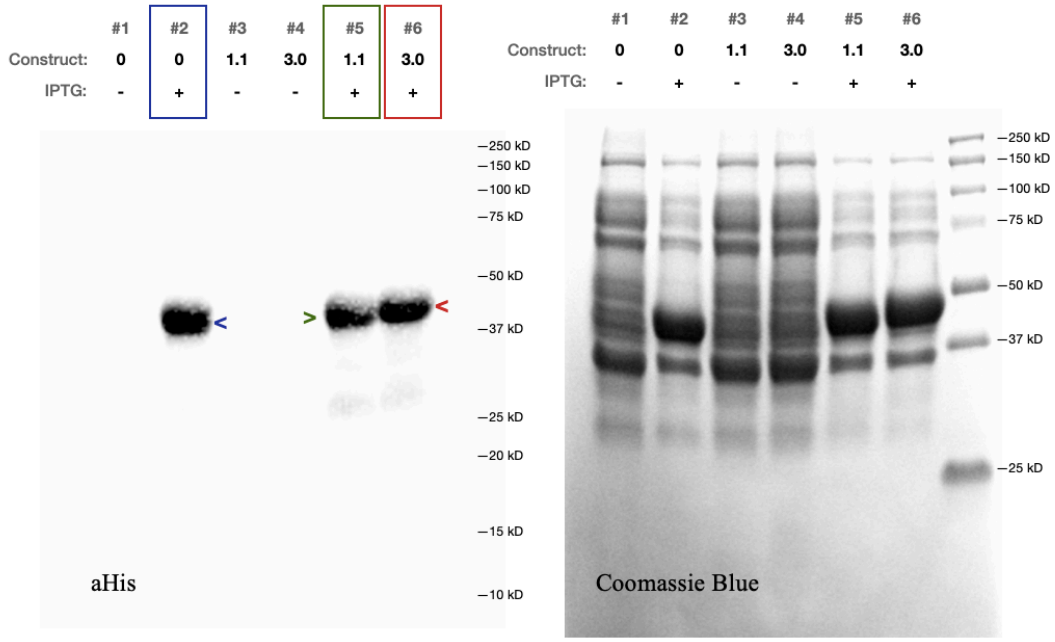

Figure 7. Expression Results of diCBM40-0, 1.1, and 3.0. Band shifting patterns are correlated with the sizes of different constructs. Western blot is shown on the left, Coomassie blue staining on the right.

successfully labeled with oligoglycine dye as expected (Figure 8. Lane #6 & #12). The construct that without LPETG tag, diCBM40-0, was not labeled with fluorophore (Figure 8. Lane #1). While the unlabeled or reacted diCBM40-0 showed up in elution fraction of the reaction on anti-His Western-Blot gel and Coomassie Blue Staining gel(Figure 8. Lane #2). Sample lane F.T.#2 (Lane #6) and F.T.#3 (Lane #12) demonstrated a very strong labeling efficiency in in-gel fluorescence, and, in this figure, no significant conjugation efficiency difference was observed between construct 1.1 and 3.0 where LPETG motifs were distanced differently from the binding region of diCBM40. Interestingly, when the triglycine dye was absent in the diCBM40-1.1 and diCBM40-3.0 reacting systems, the His tags originally engineered after the LPETG tags disappeared resulting in proteins being washed out in flow-through fractions as well, which are detectable on Coomassie Blue Staining gel, but not on anti-His Western Blot nor with in-gel fluorescence (Figure 8. Lane #8 & #14). Among all the diCBM40

constructs we engineered, construct 1.1 and 3.0 will be at the most suitable for eSrtA-mediated protein conjugation and the following cell surface glycan imaging. But before moving on to cell imaging we need to verify the binding ability and efficiency of these protein constructs.

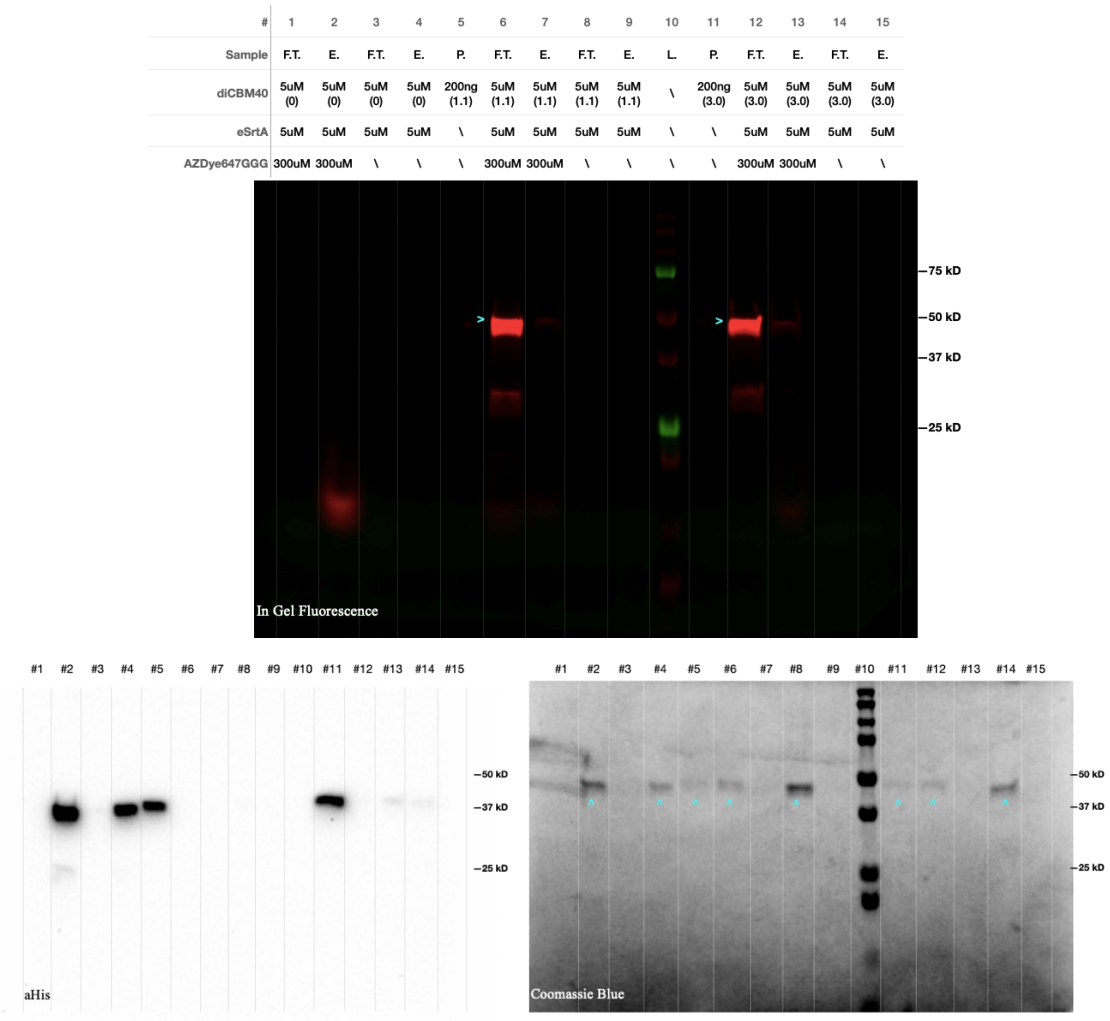

Figure 8. In gel fluorescence, anti-His western blot, and Coomassie blue staining assays of protein conjugation reaction result. Lane 1~4 are showing results with construct 0, the one without LPETG tag; lane 5~9 are showing construct 1.1 that with LPETG tag and a shorter linker sequence; lane 11~15 are showing construct 3 with LPETG tag and a longer linker sequence. F.T.: Flow Through, E.: Elution, P: Unreacted scFv-Unituxin-LPETG, L.: Ladder.

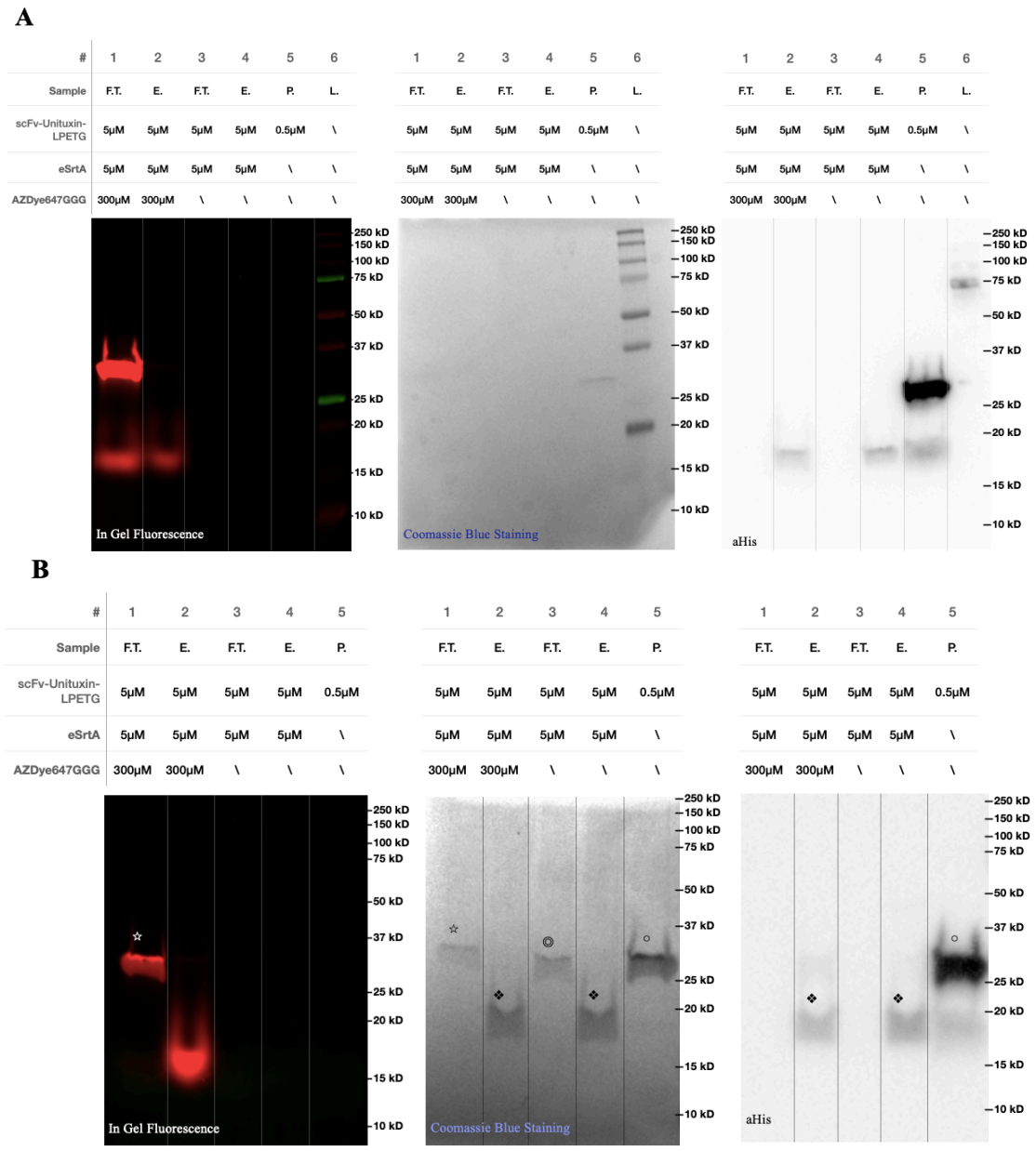

Figure 9. scFv-Unituxin-LPETG Protein Conjugation Results under the reaction condition of room temperature for 16 hours (A) and 4°C for 24 hours (B). F.T.: Flow Through, E.: Elution, P: Unreacted scFv-Unituxin-LPETG, L.: Ladder. ☆: Conjugated scFv-Unituxin-LPETG with dye, ◎: Reacted scFv-Unituxin-LPETG without dye, ○: scFv-Unituxin-LPETG(~25.9 kD), ❖: eSrtA (~17 kD).

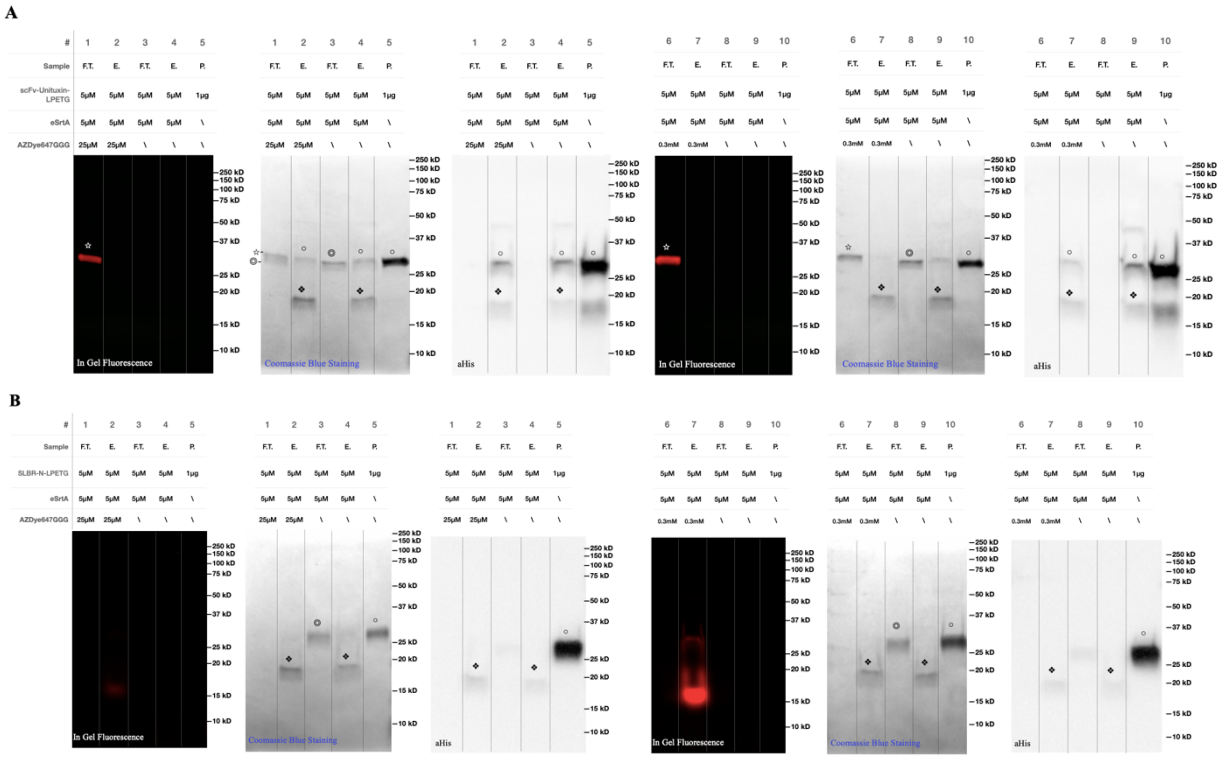

Figure 10. scFv-Unituxin-LPETG (A), and SLBR-N-LPETG (B) Protein Conjugation Results under the reaction condition of 4℃ for 24 hours with lower dye concentration (25uM, 1:5) and room temperature for 4 hours with the same dye concentration (300uM, 1:60). F.T.: Flow Through, E.: Elution, P: Unreacted scFv-Unituxin-LPETG/SLBR-N-LPETG Construct, L.: Ladder. ☆ : Conjugated scFv-Unituxin-LPETG/SLBR-N-LPETG with dye, ◎: Reacted scFv-Unituxin-LPETG/SLBR-N-LPETG without dye, ◦: scFv-Unituxin-LPETG(~25.9 kD)/SLBR-N-LPETG(~28.2 kD), ❖: eSrtA (~17 kD).

With the LPETG tag engineered to their N-termini, scFvs or SLBRs can be similarly recognized and conjugated with an oligoglycine dye by evolved sortase A. Using conventional protein analytic techniques—Coomassie blue staining, Western Blot, and in-gel fluorescence, we also can evaluate this protein conjugation efficiency. Firstly, we tested two protein conjugation conditions for scFv-Unituxin-LPETG, room temperature for 16 hours and 4℃ for 24 hours, both with 1:60 protein to dye ratio. As the results indicated (Figure 9.), this reaction is more efficient under the lower temperature. While under room temperature, although we can detect some fluorescence signal from in-gel fluorescence, the protein retrieved from the reaction system is in low

quantity as suggested in Coomassie blue staining pattern (Figure 9. A). This could be stemmed from the low stability of scFv protein in room temperature for a relatively long time. We then applied this seemingly preferred reaction condition—4℃ for 24 hours—to other proteins, scFv-BR96, SLBR-N, and SLBR-B. Unfortunately, there is no clear evidence of conjugation reaction happening for them. Interestingly, even though no fluorescence signal detected from both SLBR constructs, clear flow-through bands showed up on Coomassie blue staining gel in the lane of reaction samples that are in absence of oligoglycine dye. This provided a clue that these SLBR proteins might not be stable in the environment with concentrated dye. To test this hypothesis, we lower the dye concentration for SLBR-N-LPETG conjugation reaction. Alternatively, we tested the reaction efficiency under the room temperature for shorter time, scFv-Unituxin-LPETG was also set up in these conditions as a positive control. As shown in Figure 10., scFv-Unituxin-LPETG worked in both low-dye-concentration and shorter-time conditions, although an inefficient conjugation took place in low-dye concentration condition as two flow-through bands showed up on Coomassie blue staining gel in the lane of reaction sample containing oligoglycine dye and some unreacted protein showed up in elution lanes (Figure 10. A). On the other hand, there is still no fluorescent band detected in SLBR-N-LPETG reaction systems (Figure 10 B.), we thus believed that this commercial dye, AZDye-647-Gly-Gly-Gly, is not tolerable for SLBR proteins, since SLBR-N-LPETG has shown to be stable in 3% DMSO solution where this dye is dissolved. As for scFv-BR96-LPETG protein, we deducted that the major reason for it not being conjugated was attributed to low protein quality, since the target scFv-BR96 bands are faint in all gel images. Accordingly, we will move scFv-Unituxin-LPTEG forward to glycan target binding and cell labeling tests and expecting effective outcome, predicated by its great conjugation efficiency and DMSO tolerance. We also tried to use a different fluorophore, AZDye-488-Gly-Gly-Gly, and a adjust reaction recipe for scFv-

Unituxin. We intentionally increased the concentration of the protein, eSrtA, and fluorophore, as well as a lower protein-to-dye ratio to save material. The labeled protein is showing in Coomassie Blue Staining Gel and In-gel Fluorescence Gel with ideal molecular weight and fluorescence-emission(Figure 11. #1), sortase is recovered from column elution fraction and is showing in Coomassie Blue Staining Gel and aHis Western Blot(Figure 11. #2 & #4). The His-tag cleaved but no fluorophore labeled scFv-Unituxin is missing in the gel images(Figure 11. #3), which could be resulted from low gel loading quantities.

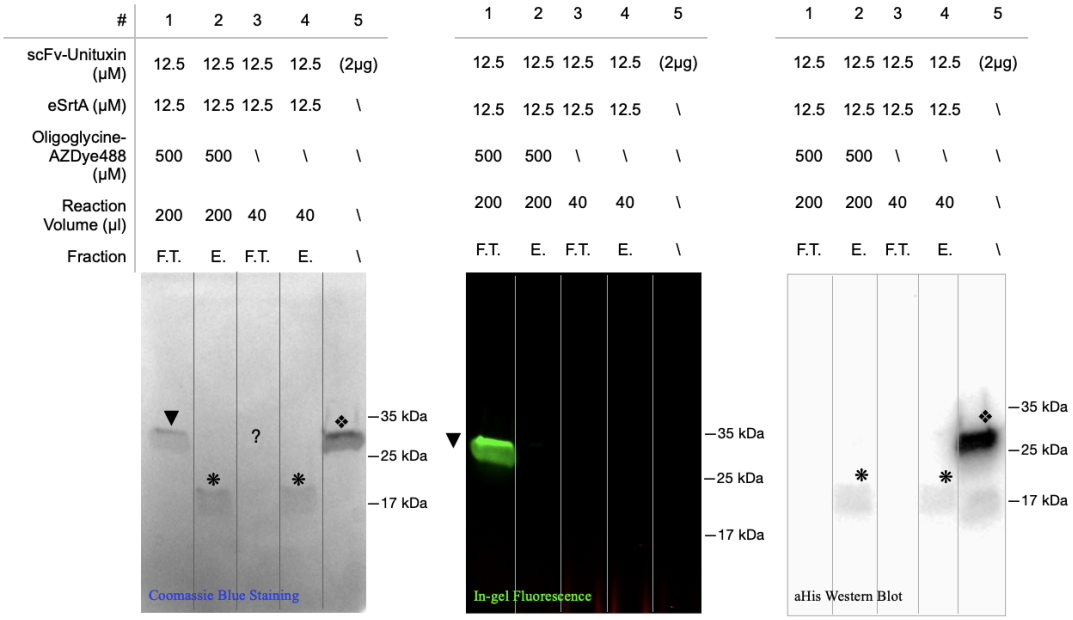

Figure 11 . Reaction Recipe and Product Gel Images for Sortase Reaction. 1:1:40 or 1:1:0 Protein to enzyme to dye ratio was used in the reactions, and the reactions was conducted under room temperature, in dark tube, for around 16 hours with rotation. Reaction product fractions were separated with Ni-NTA resin column, #1 and #3 are from column flow-through and #2 and #4 are from column elution. F.T.: Flow Through, E.: Elution. ▼: Fluorophore-Conjugated Protein (showing in Coomassie Blue Staining Gel and In-gel Fluorescence Gel); ❋: Sortase (showing in Coomassie Blue Staining Gel and aHis Western Blot); ❖: Starting Protein (showing in Coomassie Blue Staining Gel and aHis Western Blot); ?: His-tag cleaved protein is missing in the Coomassie blue staining gel.

2. Cell-Surface Antigens Binding Assay

Cell surface ELISA assay was chosen for primary binding assay and human breast epithelial cell line (MCF10A dct moxGFP-MUC1 and MCF10A dct moxGFP-MUC1 GNE KO, engineered by Paszek Lab) was chosen as our model organism. GNE gene encodes the bifunctional UDP-N-acetylglucosamine-2-epimerase/N-acetylmannosamine kinase (GNE/MNK), the key enzyme of sialic acid biosynthesis (96). By knocking out this gene, the silica acid biosynthetic pathway will be impaired. As a result, in MCF10A GNE KO cell line, no cell surface glycans with terminal N-acetylneuraminic acids will be found. From ELISA assay, we have demonstrated that diCBM40 binding to cell surface Neu5Ac or α(2,3)-sialyl-lactose is concentration dependent and three constructs we used have similar binding efficiency with construct 3.0 being slightly higher than other two (Figure 12.). We have also showed that when

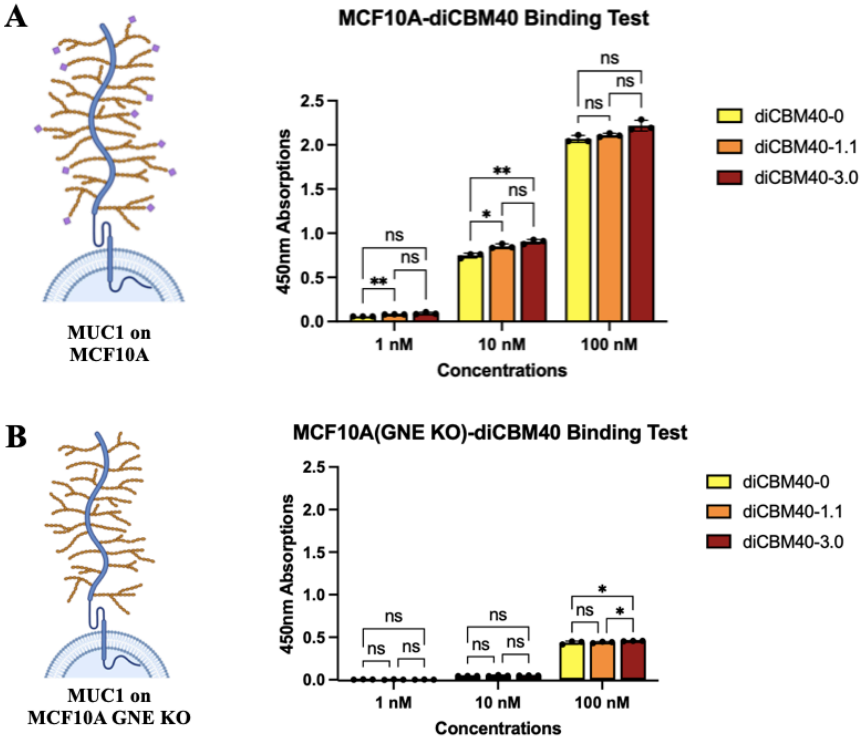

Figure 12. Cell Surface ELISA Assay for diCBM40-0, 1.1, & 3.0 with MCF10A (A) and MCF10A GNE KO (B) Cell Lines. (ns=not significant, P values>0.05; *, P values≦0.05; **, P values≦0.01; ***, P values≦0.001; ****, P values≦0.0001)

cell surface lacking Neu5Ac, the binding efficiency of diCBM40 will be significantly decreased (Figure 13.). When comparing to wheat germ agglutinin (WGA), although the binding signals for diCBM40s are clearly higher, we have to be cautious of saying that diCBM40 is a better glycan binding protein than WGA is, since the interaction bases for ELISA assay of them were different. However, based on the P-values those proteins' binding efficiency to GNE (+/-), it is safe to say that diCBM40 is better in differentiating cell surface glycans with terminal Neu5Ac.

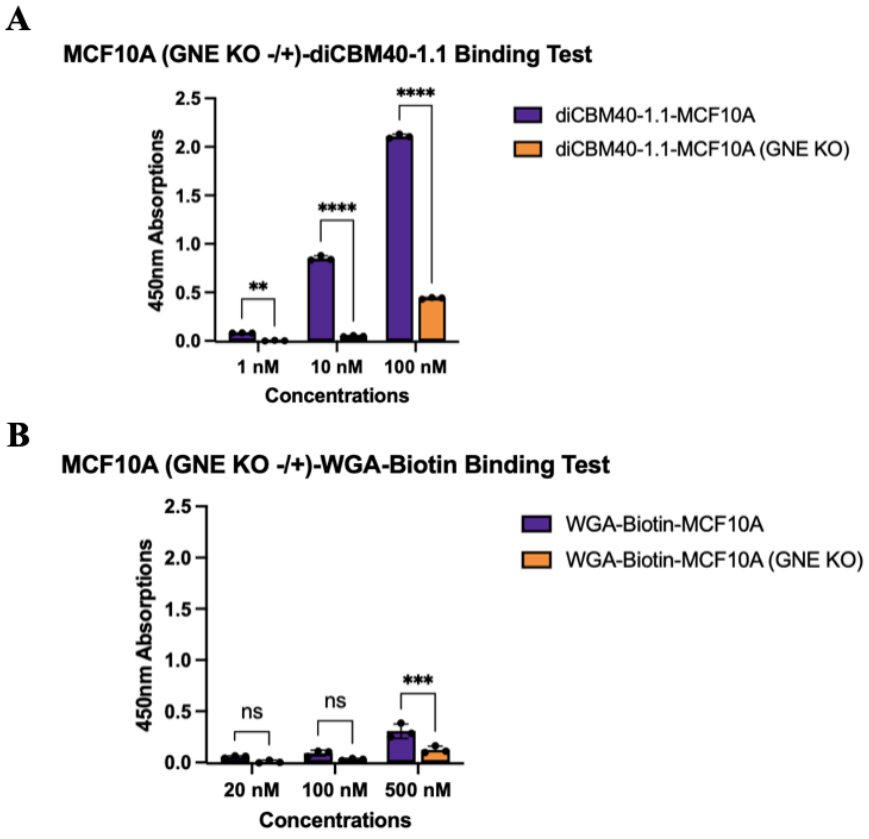

Figure 13. Cell Surface ELISA Assay for diCBM40-1.1 (A), along with biotinylated wheat germ agglutinin (WGA-Biotin) (B) with MCF10A and MCF10A GNE KO Cell Lines. (ns=not significant, P values>0.05; *, P values≦0.05; **, P values≦0.01; ***, P values≦0.001; ****, P values≦0.0001)

We then changed the binding test method to FACS. In this test, one commercialized mouse anti-GD2 full-length IgG (14.G2a) (BD Biosciences®)

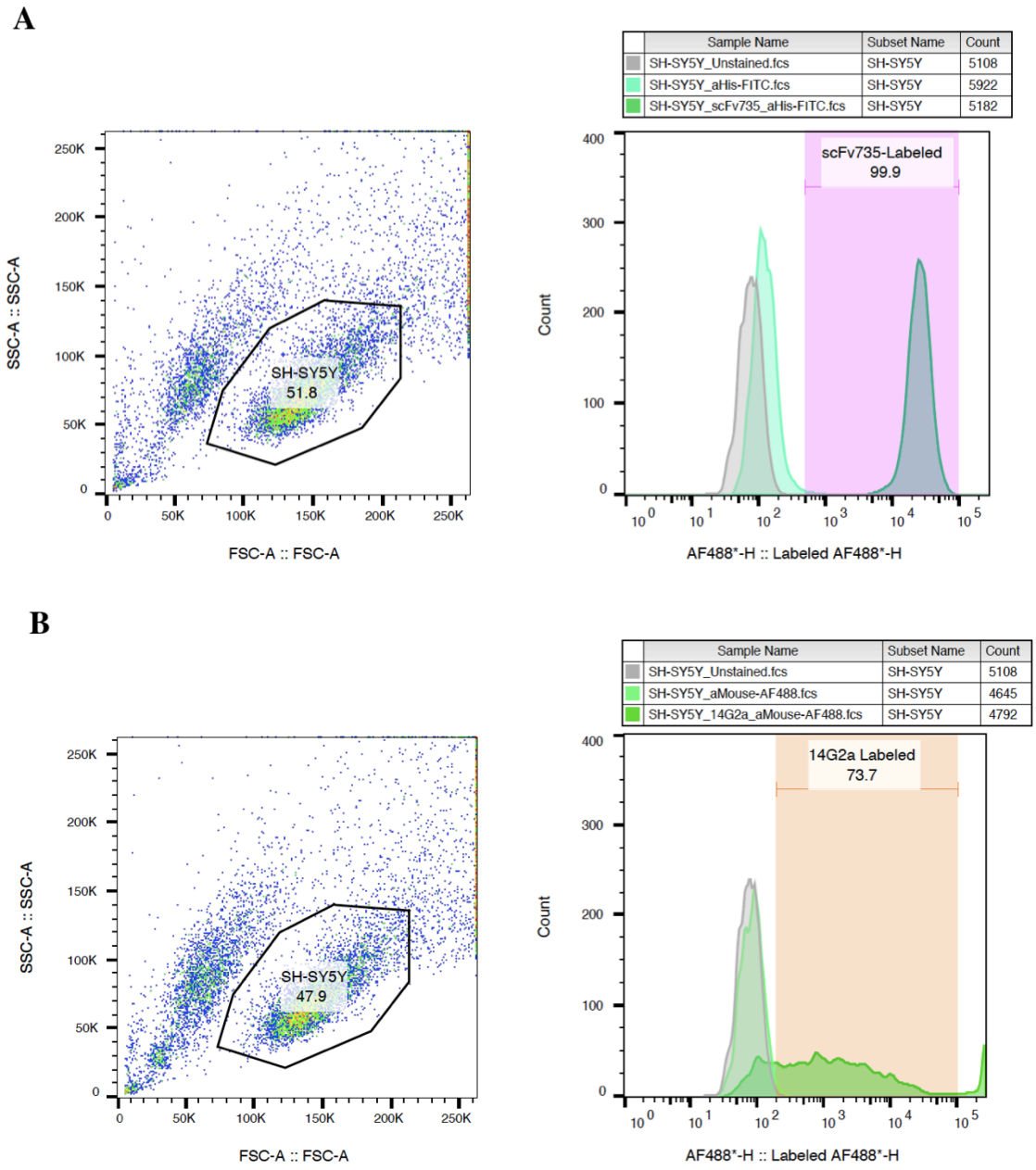

Figure 14. Fluorophore-Activated Cell Sorting (FACS) Analysis of SH-SY5Y Cell Surface Tumor-Associated Antigen Binding Tests. (A) SH-SY5Y ploy-sialic acids binding test with scFv735, aHis-FITC was used as secondary antibody; (B) SH-SY5Y GD2 binding test with commercialized 14G2a, aMouse-488 was used as secondary antibody. The gating strategies were shown on the left, respectively. 51.8% of scFv735 labeled cell population and 47.9% of 14G2a labeled cell population were selected for fluorophore emission detection.

(97~103) was used. Antibody clone 14.G2a is an isotope switch variant (IgG2a) of antibody Ch14.18 which is produced by IgG3-producing hybridoma that specially react

with human and mouse GD2 (104). The first cell model used in this test is SH-SY5Y with the presence of GD2 being reported (102~103). As shown in Figure 14, scFv735 was firstly used targeting for poly-sialic acid (Figure 14. (A)), one of the pre-established SH-SY5Y tumor-associated surface antigens. The reason for including this antigen binding test is to verify the authenticity of our cell line, as well as to test the validity of our flow cytometry cell binding protocol. Through the gating strategy shown in the figure, 99.9% of the cell culture demonstrated clean poly-sialic acid positive binding.

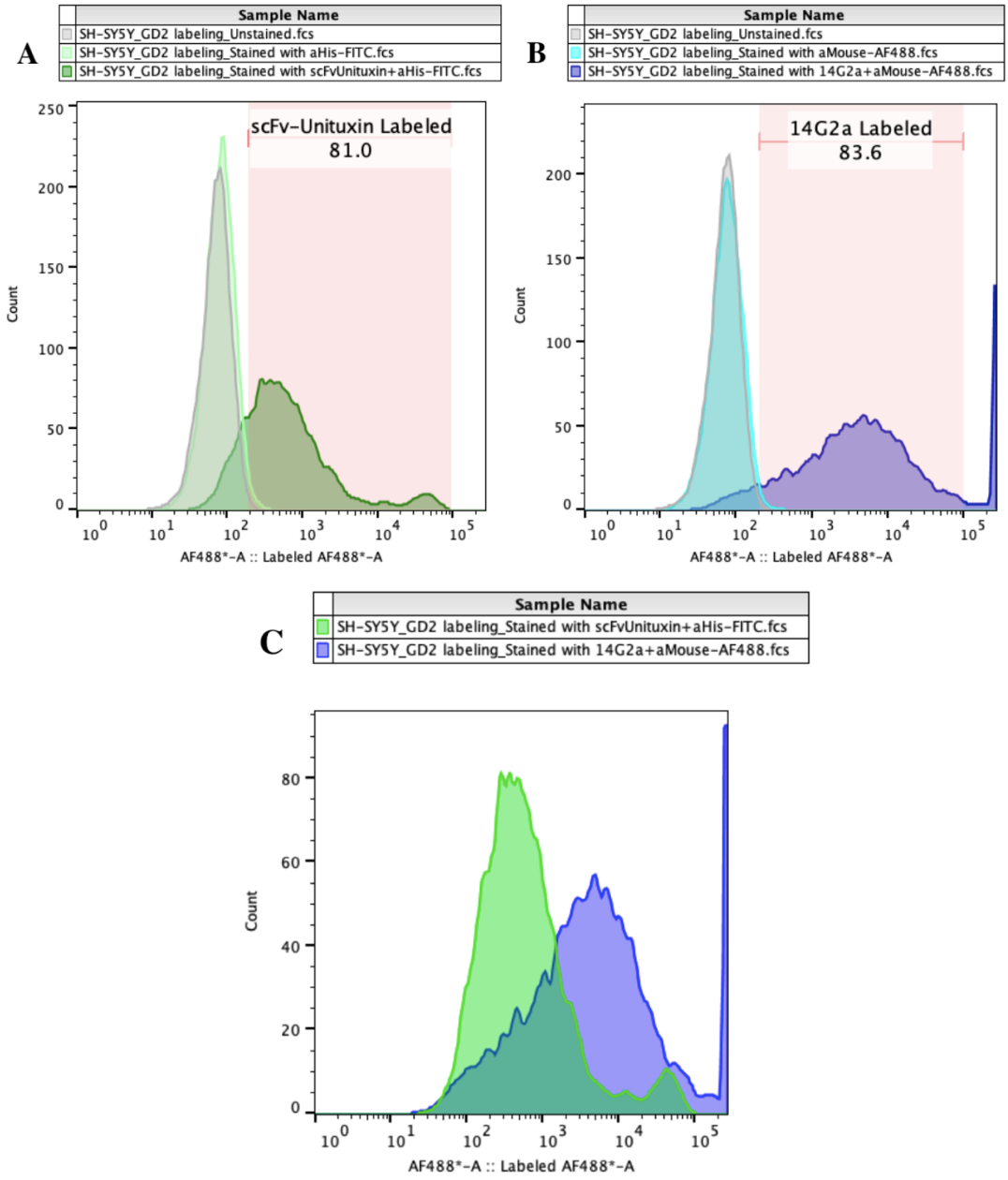

Figure 15 . Fluorophore-Activated Cell Sorting (FACS) Analysis of SH-SY5Y Cell Surface Tumor-Associated Antigen Binding Tests. (A) SH-SY5Y labeled with engineered scFv-Unituxin as primary antibody and anti-His tag FITC as secondary antibody, labeled cells are highlighted in the pink region with 81% of total count; (B) SH-SY5Y labeled with commercially acquired anti-GD2, 14G2a, as primary antibody and anti-mouse AF488 as secondary antibody, labeled cells are highlighted in the pink region with 83.6% of total count; (C) scFv-Unituxin labeled and 14G2a labeled SH-SY5Y cells in the same histogram for direct comparison.

The commercial anti-GD2 full-length IgG was then used in following (Figure 14. (B)). In the figure, we observed an inconsistency in cell labeling, or, in other words,

different cells have shown different GD2 positive signal intensities, compared to poly-sialic acid binding test. This phenomenon may have to do with the general accessibility of GD2 molecules as they are relatively short in height in comparison to other glycoproteins. When replicating our first result (Figure 15.), we also include the in-house engineered scFv-Unituxin (Figure 15. (B)). The results have shown a similar labeling pattern in 14G2a binding test and scFv-Unituxin binding test. This proved that our engineered protein obtains a comparable binding ability to the commercialized one. We then tested the binding ability of our in-house engineered scFv-Unituxin-LPETG (Figure 15. (A)). The commercial anti-GD2 full-length IgG was used in following for parallel compare (Figure 15. (B)). In the figure, both antibodies are shown being able to label the GD2 in SH-SY5Y cell surface, and we observed an inconsistency in cell labeling, or, in other words, different cells have shown different GD2 positive signal intensities, compared to previous poly-sialic acid binding test. This phenomenon may have to do with the general accessibility of GD2 molecules as they are relatively short in height in comparison to other glycoproteins. When comparing these two antibodies directly, we can see a better labeling ability for commercial antibody 14G2, and a greater consistency for engineered scFv-Unituxin, as the average signal intensity is higher in 14G2a and the range of signal intensity is narrower in scFv-Unituxin (Figure 15. (C)). This leads to the conclusion that 14G2a has a higher GD2 affinity and scFv-Unituxin has a better sensitivity for cell surface GD2. In general, despite the differences, these results have shown a similar labeling pattern in 14G2a binding test and scFv-Unituxin binding test. This proved that our engineered protein obtains a comparable binding ability to the commercialized one.

3. Cell Imaging

We scaled-up the labeling previously engineered diCBM40-1.1(LPTEG-tagged with short linker) with oligoglycine-AZDye647 (Compound 1, Click Chemistry Tools) through evolved sortase A-mediate transpeptidation, the LPETG motif can be recognized by sortase, and according to mechanism the C-terminus His tag will be cleaved out upon completion of the reaction (38), which further facilitates the separation

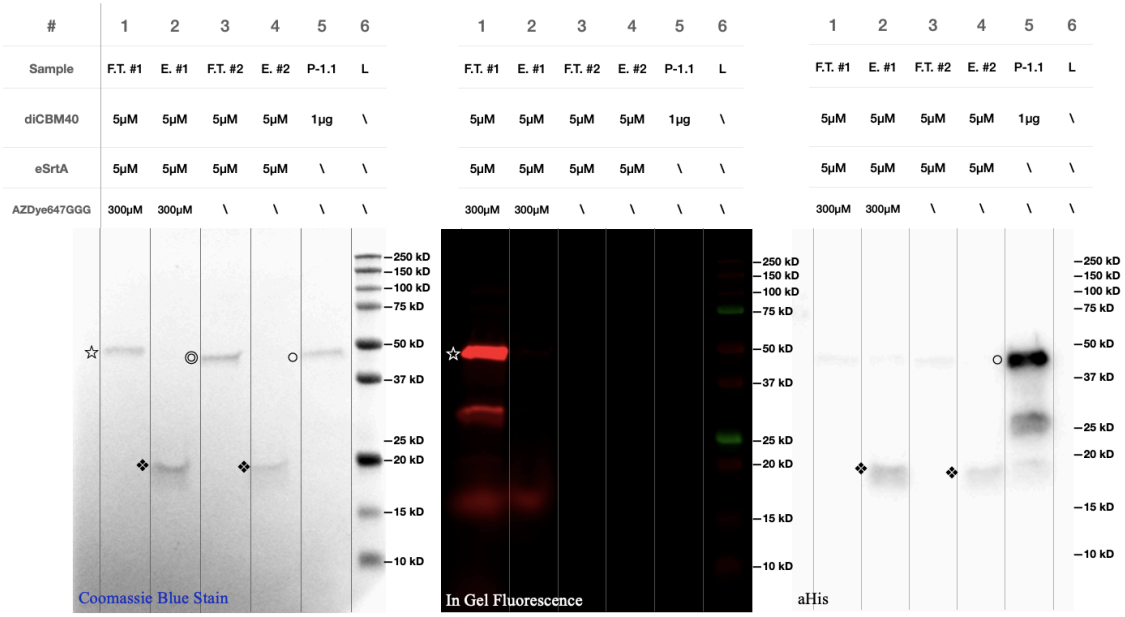

Figure 16 . Coomassie blue staining, in gel fluorescence, and western blot analysis of diCBM40-LPETG fluorophore labeling result. Reaction sample #1 was sortase-mediated conjugation of diCBM40-LPETG with oligoglycine dye, #2 was without dye. Since the His tag on conjugated protein will be cleaved out, the target product will be coming through the nickel resin which will be collected and noted as flow through. The elution fraction was also collected and analysis, so reaction efficiency can be evaluated. F.T.: Flow Through, E.: Elution, P-1.1.: Unreacted diCBM40-1.1 Construct, L.: Ladder. ☆: Conjugated diCBM40-1.1 with dye, ◎: Reacted diCBM40-1.1 without dye, ◦: diCBM40-1.1 (~45.1 kD), ❖: eSrtA (~17 kD).

of protein conjugates and unreacted proteins. After overnight labeling, the reaction product was analyzed with Coomassie blue staining, in gel fluorescence, and western blot (Figure 16.). Similar to previous result, the conjugation efficiency was proven to be strong. Lane 1 and 3 were loaded with Ni-NTA resin flow through of the reaction mixture with and without oligoglycine dye respectively, where the target fluorophore-

labeled diCBM40s were expected to be, while land 2 and 4 were loaded with Ni-NTA resin elution, which were collected to evaluate the conjugation efficiency. Comparing the flow through and elution fraction of the mixture, it is clear that almost all of the diCBM40-LPETG were labeled with fluorophore in reaction sample #1 (Figure 16., Lane #1 & #2)and that the His tag was cleaved even in absence of oligoglycine dye in reaction sample #2 (Figure 16., Lane #3 & #4). According to cell surface ELISA result, diCBM40 should be exhibiting a great glycan binding affinity and specificity.

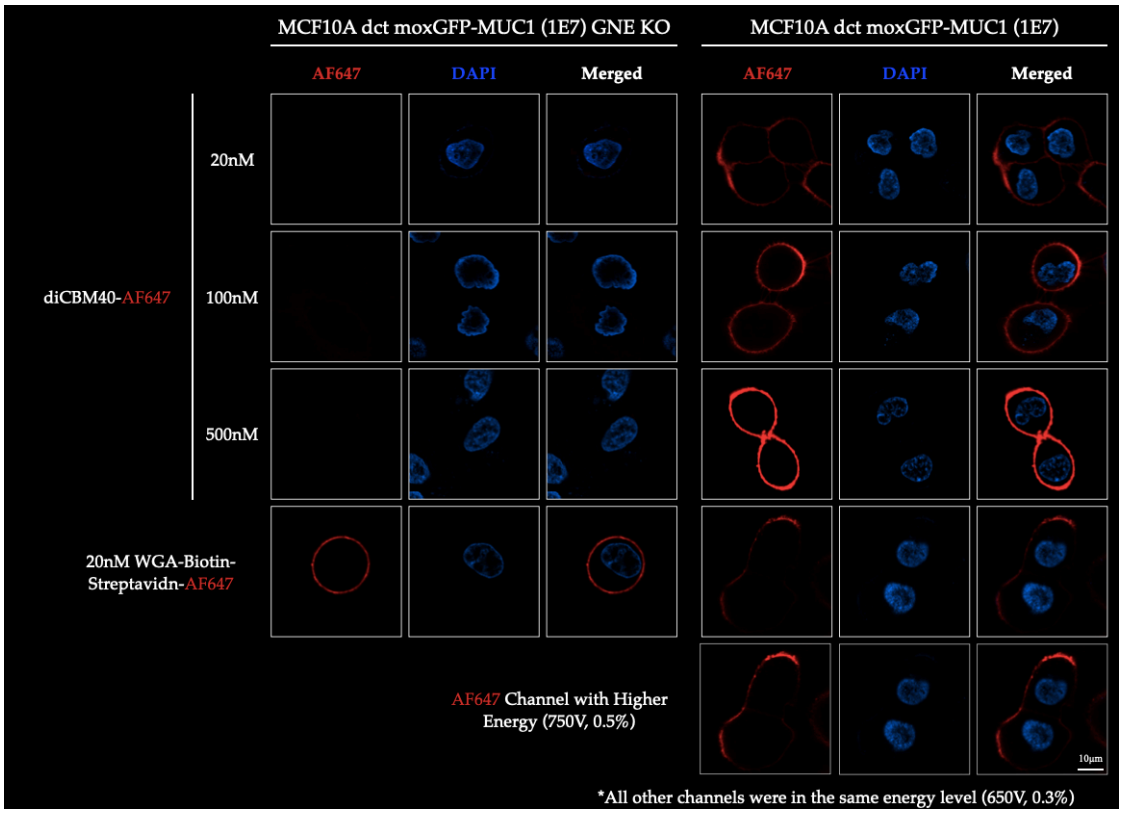

Figure 17 . Live cell imaging. MCF10A and MCF10A GNE KO cells were seeded on 35mm glass-bottom dishes with 1x104 cell/ml density;6 samples of cells were labeled with different concentrations of diCBM40-AF647 with 1x Hoechst Buffer in 0.5% BSA PBS Buffer for 1hr in dark room; 2 samples of cells were firstly labeled with Biotinylated Wheat Germ Agglutinin (WGA-Biotin) for 1hr in dark room, then labeled with Streptavidin-AF647 with 1x Hoechst Buffer in 0.5% BSA PBS Buffer for 1hr in dark room.

Live cell imaging was performed with two same cell lines as in ELISA, MCF10A dct moxGFP-MUC1 (1E7) and MCF10A dct moxGFP-MUC1 (1E7) GNE KO. The GNE KO cells were considered as negative control, as no terminal N-acetylneuraminic acid is present on cell surface glycan. As shown in figure 8, diCBM40 protein was able to label the cell surface glycan with terminal N-acetylneuraminic acid, the one on MCF10A cell, in a concentration-dependent manner (Figure 17.). As the increase of diCBM40-AF647 concentration, 647nm channel signals on MCF10A dct moxGFP-MUC1 (1E7) cells were getting stronger, whereas no strong enough signal can be detected from MCF10A dct moxGFP-MUC1 (1E7) GNE KO cells under the same condition. In comparison to wheat germ agglutinin (WGA), another glycan binding protein that binds to N-acetyl- D-glucosamine and Sialic acid, diCBM40 demonstrated a better specificity in differentiating glycan with terminal N-acetylneuraminic acid (Figure 17.). These results can be verified correspondingly with the ELISA results (Figure 13.).

IV. Conclusions and Future Perspectives

1. Conclusions of Developing a Glycan-Binding Molecular Toolkit

Here in Table 2 and Table 3 the sortase-mediated modification performances of engineered glycan-binding proteins and the tested mammalian cell lines are summarized, respectively. In conclusion, we have successfully engineered, modified, performed cell surface glycan binding assay, and cell surface glycan imaging for α(2,3)-sialyl-lactose binding diCBM40, polysialic acid binding scFv735, and GD2 binding scFv-Unituxin. They are proven to be validate glycan-study proxies that tolerate certain degree of modification to achieve glycan structural affinity and specificity in the GlycoExM technique. In terms of mammalian cell lines, human lung cancer epithelial cell line A549, human small cell lung cancer epithelial cell line SW2, human ovarian adenocarcinoma epithelial cell SKOV3, human bone neuroblastoma epithelial cell line SH-SY5Y, and human fibrocystic breast epithelial cell line MCF10A were individually cultured and tested on their expression of glycans of interest. Specifically, MCF10A will be ideal for α(2,3)-sialyl-lactose imaging, SH-SY5Y will be ideal for polysialic acids and GD2 imaging. These two cell lines will be used in expansion microscopy experiments.

2. Limitations of Conventional Glycan Imaging

Using this imaging molecular toolkit mentioned above, we are now able to identify specific glycan structures in healthy cells or cells in their disease states. However, revealing the nanoscale information of cell surface glycans, including their intermolecular association and interaction, cannot be achieved by simply lighting up the cells, which has already been accomplished by simpler conventional glycan imaging technologies (53, 54, 56~60). The field of submolecular study of cell surface glycans is still lagging largely owning to the limitations of in-cell imaging techniques. To be able

to have an in-depth understanding of the constitutions, associations, and interactions of cell surface glycans, we have to address the resolution limitation of conventional imaging techniques that prevents us to obtain cleaner and clearer images of those overcrowded glycocalyx. One of the major impediments for high resolution imaging is the diffraction-limited resolution (105) which is rooted from the comparable distances between the fluorophores or light-emitting units to visible light wavelengths, and the light diffractions in such cases will pose a barrier on the image resolutions.

3. Super-Resolution Microscopy and Its Potential in Glycan Imaging

To overcome this diffraction-limited resolution problem, almost 20 years ago, Xiaowei Zhuang's lab and Eric Betzig's lab independently, and almost simultaneously, developed technologies called stochastic optical reconstruction microscopy (STORM) (106) and photoactivated localization microscopy (PALM) (107), respectively. These two technologies shared a very similar principle in which the fluorophore labeled samples will undergo multiple rounds of imaging, and in each round only a subset of fluorophores will be stochastically activated and turned on. The fluorophores within this small set are going to be spatially distant and hence distinguishable from each other. They will then be recorded and localized before being photobleached or turned off. By repeating this procedure many times, an intact and high-resolution picture can be generated (106, 107). As revolutionary as STORM and PALM are, they impose a certain degree of complexity to the imaging procedure and the data analysis process. As a result, 10 years later, a new technique, expansion microscopy(108), was born in Edward Boyden's lab. They came up with a simple idea to achieve high resolution by expanding the imaging sample, or physically increase the distance between the light-emitting units. In doing so, diffraction problem can also be resolved. When firstly developed, expansion microscopy used a so-called DNA method (108), where the antibodies were

fused with a short sequence of DNA fragment and the fluorophore along with gel-crosslinking functional group were conjugated to another DNA fragment with the complementary sequence. After the treatment of these two elements, cell samples will be fixed and crosslinked to hydrogel, and through the gel swelling, the cell sample will also be stretched out (108). This method was then replaced by a simpler MA-NHS/GA method in which the fluorophore and the crosslinking group were directly conjugated to antibodies (109). In recent years, expansion microscopy has been further developed and used in many imaging applications. Xing Chen's group combined the expansion microscopy with metabolic labeling and bioorthogonal chemistry for lipids, glycans, DNA, RNA, and small molecules high-resolution imaging (110). Johan Hofkens's group proposed the idea of using synthetic trifunctional linker to accomplish one-step expansion microscopy for lipid membrane and cytoskeleton labeling (111). Last year, Jeremy Baskin's lab developed Lipid Expansion Microscopy (LExM) to overcome the permeability and native membrane disruption issues in the traditional ExM technologies by utilizing metabolic labeling with unnatural lipid head groups and trifunctional linkers (112). This method can well preserve the integrity of lipid membrane to obtain lipid images with not only high resolution but also high fidelity (112). In addition to biomolecule imaging, expansion microscopy has also been successfully used in unveiling detailed brain tissue structures (113).

4. Future Work in Glycan Imaging with Expansion Microscopy (GlycoExM)

Inspired by these developments in expansion microscopy, we proposed to apply similar concepts to the study of cancer cell surface glycans. We designed a synthetic trifunctional linker to conjugate the aforementioned glycan-binding proteins with hydrogel crosslinking groups and fluorophores through the same sortase-mediated modification. Specifically, the trifunctional linker molecule will contain one triglycine

peptide sequence, one azido bioorthogonal handle, and one fluorophore. With several promising glycan-binding proteins in hand, we will focus on using them to achieve high-resolution GlycoExM with the same mammalian cell lines used before in the near future.

Table 2. Glycan-Binding Protein Sortase-Mediated Modification Performances.

		diCBM40	scFv735	scFv-Unituxin	scFv-BR96	SLBR-N	SLBR-B
60x AZDye-647-GGG	R.T. 16hr	+++	+++	+	-	-	-
	R.T. 4hr	+++	+++	+++	\	-	\
	4°C 24hr	+++	+++	+++	-	-	-
5x AZDye-647-GGG	4°C 24hr	++	++	++	\	-	\
60x AZDye-488-GGG	R.T. 16hr	+++	+++	+++	\	+	+++
Dye-free Buffer	R.T. 4hr	+++	+++	+++	\	+++	\
	4°C 24hr	+++	+++	+++	-	+++	+
3% DMSO	R.T. 4hr	\	\	+++	+	+++	\
	4°C 24hr	\	\	+++	+	+++	\

No Data | No Modification | Minor Modification | Insufficient Modification | Strong Modification

Table 3. Selected Mammalian Cell Lines for Cell Surface Glycan Binding and Imaging.

Cell Line	A549	SW2	SKOV3	SH-SY5Y	MCF10A
Cell Type	Human Lung Cancer, Epithelial	Human Small Cell Lung Cancer, Epithelial	Human Ovarian Adenocarcinoma, Epithelial	Human Bone Neuroblastoma, Epithelial	Human Fibrocystic Breast Cell, Epithelial
Glycan of Interest	**GD2**; GD3; LewisY; Muc1-Tn; **Polysialic Acid**	**GD2**; LewisY; **Polysialic Acid**	LewisY; Muc1-Tn; **GD2**	**Polysialic Acid; GD2**	**α(2,3)-sialyl-lactose**

References:

1. Siegel RL, Miller KD, Wagle NS, Jemal A. Cancer statistics, 2023. CA Cancer J Clin. 2023 Jan;73(1):17-48.
2. Weller D, Vedsted P, Rubin G, Walter FM, Emery J, Scott S, Campbell C, Andersen RS, Hamilton W, Olesen F, Rose P, Nafees S, van Rijswijk E, Hiom S, Muth C, Beyer M, Neal RD. The Aarhus statement: improving design and reporting of studies on early cancer diagnosis. Br J Cancer. 2012 Mar 27;106(7):1262-7.
3. Wong KC, Chen J, Zhang J, Lin J, Yan S, Zhang S, Li X, Liang C, Peng C, Lin Q, Kwong S, Yu J. Early Cancer Detection from Multianalyte Blood Test Results. iScience. 2019 May 31;15:332-341.
4. Akinbami A, Popoola A, Adediran A, Dosunmu A, Oshinaike O, Adebola P, Ajibola S. Full blood count pattern of pre-chemotherapy breast cancer patients in Lagos, Nigeria. Caspian J Intern Med. 2013 Winter;4(1):574-9.
5. Polipalli SK, Karra VK, Jindal A, Puppala M, Singh P, Rawat K, Kapoor S. Cytogenetic Analysis for Suspected Chromosomal Abnormalities; A Five Years Experience. J Clin Diagn Res. 2016 Sep;10(9):GC01-GC05.
6. Lakhtakia R, Nema SK. Immunophenotyping of Tumours. Med J Armed Forces India. 2008 Jan;64(1):16-20.
7. Palmirotta R, Lovero D, Cafforio P, Felici C, Mannavola F, Pellè E, Quaresmini D, Tucci M, Silvestris F. Liquid biopsy of cancer: a multimodal diagnostic tool in clinical oncology. Ther Adv Med Oncol. 2018 Aug 29;10:1758835918794630.
8. Nagpal M, Singh S, Singh P, Chauhan P, Zaidi MA. Tumor markers: A diagnostic tool. Natl J Maxillofac Surg. 2016 Jan-Jun;7(1):17-20.
9. Fass L. Imaging and cancer: a review. Mol Oncol. 2008 Aug;2(2):115-52.
10. Henry NL, Hayes DF. Cancer biomarkers. Molecular oncology. 2012 Apr 1;6(2):140-6.

11. Sarhadi VK, Armengol G. Molecular Biomarkers in Cancer. Biomolecules. 2022 Jul 23;12(8):1021.
12. Zinn S, Vazquez-Lombardi R, Zimmermann C, Sapra P, Jermutus L, Christ D. Advances in antibody-based therapy in oncology. Nat Cancer. 2023 Feb;4(2):165-180.
13. Kreutzfeldt J, Rozeboom B, Dey N, De P. The trastuzumab era: current and upcoming targeted HER2+ breast cancer therapies. Am J Cancer Res. 2020 Apr 1;10(4):1045-1067.
14. Garcia J, Hurwitz HI, Sandler AB, Miles D, Coleman RL, Deurloo R, Chinot OL. Bevacizumab (Avastin®) in cancer treatment: A review of 15 years of clinical experience and future outlook. Cancer Treat Rev. 2020 Jun;86:102017.
15. Lu LL, Suscovich TJ, Fortune SM, Alter G. Beyond binding: antibody effector functions in infectious diseases. Nat Rev Immunol. 2018 Jan;18(1):46-61.
16. Wang W, Erbe AK, Hank JA, Morris ZS, Sondel PM. NK Cell-Mediated Antibody-Dependent Cellular Cytotoxicity in Cancer Immunotherapy. Front Immunol. 2015 Jul 27;6:368.
17. Weiskopf K, Weissman IL. Macrophages are critical effectors of antibody therapies for cancer. MAbs. 2015;7(2):303-10.
18. Golay J, Taylor RP. The Role of Complement in the Mechanism of Action of Therapeutic Anti-Cancer mAbs. Antibodies (Basel). 2020 Oct 28;9(4):58.
19. Zhang J, Xiao X, Liu W, Demirci G, Li XC. Inhibitory receptors of the immune system: functions and therapeutic implications. Cell Mol Immunol. 2009 Dec;6(6):407-14.
20. Brunet JF, Denizot F, Luciani MF, Roux-Dosseto M, Suzan M, Mattei MG, Golstein P. A new member of the immunoglobulin superfamily--CTLA-4. Nature. 1987 Jul 16-22;328(6127):267-70.

21. Krummel MF, Allison JP. CD28 and CTLA-4 have opposing effects on the response of T cells to stimulation. J Exp Med. 1995 Aug 1;182(2):459-65.
22. Doroshow DB, Bhalla S, Beasley MB, Sholl LM, Kerr KM, Gnjatic S, Wistuba II, Rimm DL, Tsao MS, Hirsch FR. PD-L1 as a biomarker of response to immune-checkpoint inhibitors. Nat Rev Clin Oncol. 2021 Jun;18(6):345-362.
23. Kwok G, Yau TC, Chiu JW, Tse E, Kwong YL. Pembrolizumab (Keytruda). Hum Vaccin Immunother. 2016 Nov;12(11):2777-2789.
24. Smith KM, Desai J. Nivolumab for the treatment of colorectal cancer. Expert Rev Anticancer Ther. 2018 Jul;18(7):611-618.
25. Migden MR, Rischin D, Schmults CD, Guminski A, Hauschild A, Lewis KD, Chung CH, Hernandez-Aya L, Lim AM, Chang ALS, Rabinowits G, Thai AA, Dunn LA, Hughes BGM, Khushalani NI, Modi B, Schadendorf D, Gao B, Seebach F, Li S, Li J, Mathias M, Booth J, Mohan K, Stankevich E, Babiker HM, Brana I, Gil-Martin M, Homsi J, Johnson ML, Moreno V, Niu J, Owonikoko TK, Papadopoulos KP, Yancopoulos GD, Lowy I, Fury MG. PD-1 Blockade with Cemiplimab in Advanced Cutaneous Squamous-Cell Carcinoma. N Engl J Med. 2018 Jul 26;379(4):341-351.
26. Herbst RS, Giaccone G, de Marinis F, Reinmuth N, Vergnenegre A, Barrios CH, Morise M, Felip E, Andric Z, Geater S, Özgüroğlu M, Zou W, Sandler A, Enquist I, Komatsubara K, Deng Y, Kuriki H, Wen X, McCleland M, Mocci S, Jassem J, Spigel DR. Atezolizumab for First-Line Treatment of PD-L1-Selected Patients with NSCLC. N Engl J Med. 2020 Oct 1;383(14):1328-1339.
27. Powles T, Park SH, Voog E, Caserta C, Valderrama BP, Gurney H, Kalofonos H, Radulović S, Demey W, Ullén A, Loriot Y, Sridhar SS, Tsuchiya N, Kopyltsov E, Sternberg CN, Bellmunt J, Aragon-Ching JB, Petrylak DP, Laliberte R, Wang J, Huang B, Davis C, Fowst C, Costa N, Blake-Haskins JA, di Pietro A, Grivas P.

Avelumab Maintenance Therapy for Advanced or Metastatic Urothelial Carcinoma. N Engl J Med. 2020 Sep 24;383(13):1218-1230.

28. Antonia SJ, Villegas A, Daniel D, Vicente D, Murakami S, Hui R, Yokoi T, Chiappori A, Lee KH, de Wit M, Cho BC, Bourhaba M, Quantin X, Tokito T, Mekhail T, Planchard D, Kim YC, Karapetis CS, Hiret S, Ostoros G, Kubota K, Gray JE, Paz-Ares L, de Castro Carpeño J, Wadsworth C, Melillo G, Jiang H, Huang Y, Dennis PA, Özgüroğlu M; PACIFIC Investigators. Durvalumab after Chemoradiotherapy in Stage III Non-Small-Cell Lung Cancer. N Engl J Med. 2017 Nov 16;377(20):1919-1929.
29. Youssef G, Dietrich J. Ipilimumab: an investigational immunotherapy for glioblastoma. Expert Opin Investig Drugs. 2020 Nov;29(11):1187-1193.
30. Keam SJ. Tremelimumab: First Approval. Drugs. 2023 Jan;83(1):93-102.
31. Sharma P, Allison JP. The future of immune checkpoint therapy. Science. 2015 Apr 3;348(6230):56-61.
32. Varki A, Cummings RD, Esko JD, et al., editors. Essentials of Glycobiology [Internet]. 4th edition. Cold Spring Harbor (NY): Cold Spring Harbor Laboratory Press; 2022.
33. Ajit Varki, Biological roles of glycans, Glycobiology, Volume 27, Issue 1, 1 January 2017, Pages 3-49.
34. Lee-Sundlov MM, Stowell SR, Hoffmeister KM. Multifaceted role of glycosylation in transfusion medicine, platelets, and red blood cells. J Thromb Haemost. 2020 Jul;18(7):1535-1547.
35. Schnaar RL. Glycobiology simplified: diverse roles of glycan recognition in inflammation. J Leukoc Biol. 2016 Jun;99(6):825-38.

36. Xiao H, Woods EC, Vukojicic P, Bertozzi CR. Precision glycocalyx editing as a strategy for cancer immunotherapy. Proc Natl Acad Sci U S A. 2016 Sep 13;113(37):10304-9.
37. Gray MA, Stanczak MA, Mantuano NR, Xiao H, Pijnenborg JFA, Malaker SA, Miller CL, Weidenbacher PA, Tanzo JT, Ahn G, Woods EC, L√§ubli H, Bertozzi CR. Targeted glycan degradation potentiates the anticancer immune response in vivo. Nat Chem Biol. 2020 Dec;16(12):1376-1384.
38. Rodrigues E, Macauley MS. Hypersialylation in Cancer: Modulation of Inflammation and Therapeutic Opportunities. Cancers (Basel). 2018 Jun 18;10(6):207.
39. Smith BAH, Bertozzi CR. The clinical impact of glycobiology: targeting selectins, Siglecs and mammalian glycans. Nat Rev Drug Discov. 2021 Mar;20(3):217-243.
40. Flynn RA, Pedram K, Malaker SA, Batista PJ, Smith BAH, Johnson AG, George BM, Majzoub K, Villalta PW, Carette JE, Bertozzi CR. Small RNAs are modified with N-glycans and displayed on the surface of living cells. Cell. 2021 Jun 10;184(12):3109-3124.e22.
41. Fuster MM, Esko JD. The sweet and sour of cancer: glycans as novel therapeutic targets. Nat Rev Cancer. 2005 Jul;5(7):526-42.
42. Hudak JE, Bertozzi CR. Glycotherapy: new advances inspire a reemergence of glycans in medicine. Chem Biol. 2014 Jan 16;21(1):16-37.
43. Pinho SS, Reis CA. Glycosylation in cancer: mechanisms and clinical implications. Nat Rev Cancer. 2015 Sep;15(9):540-55.
44. Paszek MJ, DuFort CC, Rossier O, Bainer R, Mouw JK, Godula K, Hudak JE, Lakins JN, Wijekoon AC, Cassereau L, Rubashkin MG, Magbanua MJ, Thorn KS, Davidson MW, Rugo HS, Park JW, Hammer DA, Giannone G, Bertozzi CR,

Weaver VM. The cancer glycocalyx mechanically primes integrin-mediated growth and survival. Nature. 2014 Jul 17;511(7509):319-25.

45. Grzesik K, Janik M, Hoja-Łukowicz D. The hidden potential of glycomarkers: Glycosylation studies in the service of cancer diagnosis and treatment. Biochim Biophys Acta Rev Cancer. 2023 Mar 29:188889.
46. Pearce OM, Laubli H. Sialic acids in cancer biology and immunity. Glycobiology. 2016 Feb;26(2):111-28.
47. Schultz MJ, Swindall AF, Bellis SL. Regulation of the metastatic cell phenotype by sialylated glycans. Cancer Metastasis Rev. 2012 Dec;31(3-4):501-18.
48. Kannagi R, Sakuma K, Miyazaki K, Lim KT, Yusa A, Yin J, Izawa M. Altered expression of glycan genes in cancers induced by epigenetic silencing and tumor hypoxia: clues in the ongoing search for new tumor markers. Cancer Sci. 2010 Mar;101(3):586-93.
49. Bull C, Stoel MA, den Brok MH, Adema GJ. Sialic acids sweeten a tumor's life. Cancer Res. 2014 Jun 15;74(12):3199-204.
50. Hudak JE, Canham SM, Bertozzi CR. Glycocalyx engineering reveals a Siglec-based mechanism for NK cell immunoevasion. Nat Chem Biol. 2014 Jan;10(1):69-75.
51. Jandus C, Boligan KF, Chijioke O, Liu H, Dahlhaus M, Démoulins T, Schneider C, Wehrli M, Hunger RE, Baerlocher GM, Simon HU, Romero P, Münz C, von Gunten S. Interactions between Siglec-7/9 receptors and ligands influence NK cell-dependent tumor immunosurveillance. J Clin Invest. 2014 Apr;124(4):1810-20.
52. Xiao H, Woods EC, Vukojicic P, Bertozzi CR. Precision glycocalyx editing as a strategy for cancer immunotherapy. Proc Natl Acad Sci U S A. 2016 Sep 13;113(37):10304-9.

53. Ward EM, Kizer ME, Imperiali B. Strategies and Tactics for the Development of Selective Glycan-Binding Proteins. ACS Chem Biol. 2021 Oct 15;16(10):1795-1813.
54. Wisnovsky S, Bertozzi CR. Reading the glyco-code: New approaches to studying protein-carbohydrate interactions. Curr Opin Struct Biol. 2022 Aug;75:102395
55. Mahal LK, Yarema KJ, Bertozzi CR. Engineering chemical reactivity on cell surfaces through oligosaccharide biosynthesis. Science. 1997 May 16;276(5315):1125-8.
56. Saxon E, Bertozzi CR. Cell surface engineering by a modified Staudinger reaction. Science. 2000 Mar 17;287(5460):2007-10.
57. Baskin JM, Prescher JA, Laughlin ST, Agard NJ, Chang PV, Miller IA, Lo A, Codelli JA, Bertozzi CR. Copper-free click chemistry for dynamic in vivo imaging. Proc Natl Acad Sci U S A. 2007 Oct 23;104(43):16793-7.
58. Laughlin ST, Baskin JM, Amacher SL, Bertozzi CR. In vivo imaging of membrane-associated glycans in developing zebrafish. Science. 2008 May 2;320(5876):664-7.
59. Laughlin ST, Bertozzi CR. Imaging the glycome. Proc Natl Acad Sci U S A. 2009 Jan 6;106(1):12-7.
60. Bertozzi CR, Kiessling LL. Chemical glycobiology. Science. 2001 Mar 23;291(5512):2357-64.
61. Bourne Y, Henrissat B. Glycoside hydrolases and glycosyltransferases: families and functional modules. Curr Opin Struct Biol. 2001 Oct;11(5):593-600.
62. Owen CD, Tailford LE, Monaco S, ≈†uligoj T, Vaux L, Lallement R, Khedri Z, Yu H, Lecointe K, Walshaw J, Tribolo S, Horrex M, Bell A, Chen X, Taylor GL, Varki A, Angulo J, Juge N. Unravelling the specificity and mechanism of sialic acid recognition by the gut symbiont Ruminococcus gnavus. Nat Commun. 2017 Dec 19;8(1):2196.

63. Ribeiro JP, Pau W, Pifferi C, Renaudet O, Varrot A, Mahal LK, Imberty A. Characterization of a high-affinity sialic acid-specific CBM40 from Clostridium perfringens and engineering of a divalent form. Biochem J. 2016 Jul 15;473(14):2109-18.
64. Moustafa I, Connaris H, Taylor M, Zaitsev V, Wilson JC, Kiefel MJ, von Itzstein M, Taylor G. Sialic acid recognition by Vibrio cholerae neuraminidase. J Biol Chem. 2004 Sep 24;279(39):40819-26.
65. Connaris H, Crocker PR, Taylor GL. Enhancing the receptor affinity of the sialic acid-binding domain of Vibrio cholerae sialidase through multivalency. J Biol Chem. 2009 Mar 13;284(11):7339-51.
66. Popp MW, Antos JM, Grotenbreg GM, Spooner E, Ploegh HL. Sortagging: a versatile method for protein labeling. Nat Chem Biol. 2007 Nov;3(11):707-8.
67. Schneewind O, Model P, Fischetti VA. Sorting of protein A to the staphylococcal cell wall. Cell. 1992 Jul 24;70(2):267-81.
68. Schneewind O, Mihaylova-Petkov D, Model P. Cell wall sorting signals in surface proteins of gram-positive bacteria. EMBO J. 1993 Dec;12(12):4803-11.
69. Schneewind O, Fowler A, Faull KF. Structure of the cell wall anchor of surface proteins in Staphylococcus aureus. Science. 1995 Apr 7;268(5207):103-6.
70. Mazmanian SK, Liu G, Ton-That H, Schneewind O. Staphylococcus aureus sortase, an enzyme that anchors surface proteins to the cell wall. Science. 1999 Jul 30;285(5428):760-3.
71. Ton-That H, Liu G, Mazmanian SK, Faull KF, Schneewind O. Purification and characterization of sortase, the transpeptidase that cleaves surface proteins of Staphylococcus aureus at the LPXTG motif. Proc Natl Acad Sci U S A. 1999 Oct 26;96(22):12424-9.

72. Guimaraes CP, Witte MD, Theile CS, Bozkurt G, Kundrat L, Blom AE, Ploegh HL. Site-specific C-terminal and internal loop labeling of proteins using sortase-mediated reactions. Nat Protoc. 2013 Sep;8(9):1787-99.
73. Mao H, Hart SA, Schink A, Pollok BA. Sortase-mediated protein ligation: a new method for protein engineering. J Am Chem Soc. 2004 Mar 10;126(9):2670-1.
74. Parthasarathy R, Subramanian S, Boder ET. Sortase A as a novel molecular "stapler" for sequence-specific protein conjugation. Bioconjug Chem. 2007 Mar-Apr;18(2):469-76.
75. Ton-That H, Mazmanian SK, Faull KF, Schneewind O. Anchoring of surface proteins to the cell wall of Staphylococcus aureus. Sortase catalyzed in vitro transpeptidation reaction using LPXTG peptide and NH(2)-Gly(3) substrates. J Biol Chem. 2000 Mar 31;275(13):9876-81.
76. Popp MW, Antos JM, Grotenbreg GM, Spooner E, Ploegh HL. Sortagging: a versatile method for protein labeling. Nat Chem Biol. 2007 Nov;3(11):707-8.
77. Wagner K, Kwakkenbos MJ, Claassen YB, Maijoor K, Bohne M, van der Sluijs KF, Witte MD, van Zoelen DJ, Cornelissen LA, Beaumont T, Bakker AQ, Ploegh HL, Spits H. Bispecific antibody generated with sortase and click chemistry has broad antiinfluenza virus activity. Proc Natl Acad Sci U S A. 2014 Nov 25;111(47):16820-5.
78. Ilangovan U, Ton-That H, Iwahara J, Schneewind O, Clubb RT. Structure of sortase, the transpeptidase that anchors proteins to the cell wall of Staphylococcus aureus. Proc Natl Acad Sci U S A. 2001 May 22;98(11):6056-61.
79. Kruger RG, Otvos B, Frankel BA, Bentley M, Dostal P, McCafferty DG. Analysis of the substrate specificity of the Staphylococcus aureus sortase transpeptidase SrtA. Biochemistry. 2004 Feb 17;43(6):1541-51.

80. Naik MT, Suree N, Ilangovan U, Liew CK, Thieu W, Campbell DO, Clemens JJ, Jung ME, Clubb RT. Staphylococcus aureus Sortase A transpeptidase. Calcium promotes sorting signal binding by altering the mobility and structure of an active site loop. J Biol Chem. 2006 Jan 20;281(3):1817-26.
81. Hirakawa H, Ishikawa S, Nagamune T. Design of Ca2+-independent Staphylococcus aureus sortase A mutants. Biotechnol Bioeng. 2012 Dec;109(12):2955-61.
82. Chen I, Dorr BM, Liu DR. A general strategy for the evolution of bond-forming enzymes using yeast display. Proc Natl Acad Sci U S A. 2011 Jul 12;108(28):11399-404.
83. Kocer I, Cox EC, DeLisa MP, Celik E. Effects of variable domain orientation on anti-HER2 single-chain variable fragment antibody expressed in the Escherichia coli cytoplasm. Biotechnol Prog. 2021 Mar;37(2):e3102.
84. Holliger P, Hudson PJ. Engineered antibody fragments and the rise of single domains. Nat Biotechnol. 2005 Sep;23(9):1126-36.
85. Bird RE, Hardman KD, Jacobson JW, Johnson S, Kaufman BM, Lee SM, Lee T, Pope SH, Riordan GS, Whitlow M. Single-chain antigen-binding proteins. Science. 1988 Oct 21;242(4877):423-6.
86. Huston JS, Levinson D, Mudgett-Hunter M, Tai MS, Novotn J, Margolies MN, Ridge RJ, Bruccoleri RE, Haber E, Crea R, et al. Protein engineering of antibody binding sites: recovery of specific activity in an anti-digoxin single-chain Fv analogue produced in Escherichia coli. Proc Natl Acad Sci U S A. 1988 Aug;85(16):5879-83.
87. Riano-Umbarila L, Rojas-Trejo VM, Romero-Moreno JA, Costas M, Utrera-Espndola I, Olamendi-Portugal T, Possani LD, Becerril B. Comparative assessment

of the VH-VL and VL-VH orientations of single-chain variable fragments of scorpion toxin-neutralizing antibodies. Mol Immunol. 2020 Apr 29;122:141-147.

88. Westwood JA, Murray WK, Trivett M, Haynes NM, Solomon B, Mileshkin L, Ball D, Michael M, Burman A, Mayura-Guru P, Trapani JA, Peinert S, Honemann D, Miles Prince H, Scott AM, Smyth MJ, Darcy PK, Kershaw MH. The Lewis-Y carbohydrate antigen is expressed by many human tumors and can serve as a target for genetically redirected T cells despite the presence of soluble antigen in serum. J Immunother. 2009 Apr;32(3):292-301.
89. Garrigues J, Anderson J, Hellstrom KE, Hellstrom I. Anti-tumor antibody BR96 blocks cell migration and binds to a lysosomal membrane glycoprotein on cell surface microspikes and ruffled membranes. J Cell Biol. 1994 Apr;125(1):129-42.
90. Ly S, Anand V, El-Dana F, Nguyen K, Cai Y, Cai S, Piwnica-Worms H, Tripathy D, Sahin AA, Andreeff M, Battula VL. Anti-GD2 antibody dinutuximab inhibits triple-negative breast tumor growth by targeting GD2+ breast cancer stem-like cells. J Immunother Cancer. 2021 Mar;9(3):e001197.
91. Keyel ME, Reynolds CP. Spotlight on dinutuximab in the treatment of high-risk neuroblastoma: development and place in therapy. Biologics. 2018 Dec 21;13:1-12.
92. Nazha B, Inal C, Owonikoko TK. Disialoganglioside GD2 Expression in Solid Tumors and Role as a Target for Cancer Therapy. Front Oncol. 2020 Jul 7;10:1000.
93. Park JR, Eggert A, Caron H. Neuroblastoma: biology, prognosis, and treatment. Pediatr Clin North Am. 2008 Feb;55(1):97-120, x.
94. Bensing BA, Li Q, Park D, Lebrilla CB, Sullam PM. Streptococcal Siglec-like adhesins recognize different subsets of human plasma glycoproteins: implications for infective endocarditis. Glycobiology. 2018 Aug 1;28(8):601-611.

95. Bensing, B.A., Stubbs, H.E., Agarwal, R. et al. Origins of glycan selectivity in streptococcal Siglec-like adhesins suggest mechanisms of receptor adaptation. Nat Commun 13, 2753 (2022).

96. Nieto-Garcia O, Wratil PR, Nguyen LD, Bohrsch V, Hinderlich S, Reutter W, Hackenberger CPR. Inhibition of the key enzyme of sialic acid biosynthesis by C6-Se modified N-acetylmannosamine analogs. Chem Sci. 2016 Jun 1;7(6):3928-3933.

97. Yoshida S, Fukumoto S, Kawaguchi H, Sato S, Ueda R, Furukawa K. Ganglioside G(D2) in small cell lung cancer cell lines: enhancement of cell proliferation and mediation of apoptosis. Cancer Res. 2001 May 15;61(10):4244-52.

98. Mujoo K, Cheresh DA, Yang HM, Reisfeld RA. Disialoganglioside GD2 on human neuroblastoma cells: target antigen for monoclonal antibody-mediated cytolysis and suppression of tumor growth. Cancer Res. 1987 Feb 15;47(4):1098-104.

99. Cheresh DA, Rosenberg J, Mujoo K, Hirschowitz L, Reisfeld RA. Biosynthesis and expression of the disialoganglioside GD2, a relevant target antigen on small cell lung carcinoma for monoclonal antibody-mediated cytolysis. Cancer Res. 1986 Oct;46(10):5112-8.

100. Cheresh DA, Harper JR, Schulz G, Reisfeld RA. Localization of the gangliosides GD2 and GD3 in adhesion plaques and on the surface of human melanoma cells. Proc Natl Acad Sci U S A. 1984 Sep;81(18):5767-71.

101. Mueller BM, Romerdahl CA, Gillies SD, Reisfeld RA. Enhancement of antibody-dependent cytotoxicity with a chimeric anti-GD2 antibody. J Immunol. 1990 Feb 15;144(4):1382-6.

102. Prapa M, Caldrer S, Spano C, Bestagno M, Golinelli G, Grisendi G, Petrachi T, Conte P, Horwitz EM, Campana D, Paolucci P, Dominici M. A novel anti-GD2/4-1BB chimeric antigen receptor triggers neuroblastoma cell killing. Oncotarget. 2015 Sep 22;6(28):24884-94.

103. Sorokin M, Kholodenko I, Kalinovsky D, Shamanskaya T, Doronin I, Konovalov D, Mironov A, Kuzmin D, Nikitin D, Deyev S, Buzdin A, Kholodenko R. RNA Sequencing-Based Identification of Ganglioside GD2-Positive Cancer Phenotype. Biomedicines. 2020 May 30;8(6):142.

104. Mujoo K, Kipps TJ, Yang HM, Cheresh DA, Wargalla U, Sander DJ, Reisfeld RA. Functional properties and effect on growth suppression of human neuroblastoma tumors by isotype switch variants of monoclonal antiganglioside GD2 antibody 14.18. Cancer Res. 1989 Jun 1;49(11):2857-61.

105. Born, M., Wolf, E., Bhatia, A., Clemmow, P., Gabor, D., Stokes, A., . . . Wilcock, W. (1999). Principles of Optics: Electromagnetic Theory of Propagation, Interference and Diffraction of Light (7th ed.). Cambridge: Cambridge University Press.

106. Rust MJ, Bates M, Zhuang X. Sub-diffraction-limit imaging by stochastic optical reconstruction microscopy (STORM). Nat Methods. 2006 Oct;3(10):793-5.

107. Betzig E, Patterson GH, Sougrat R, Lindwasser OW, Olenych S, Bonifacino JS, Davidson MW, Lippincott-Schwartz J, Hess HF. Imaging intracellular fluorescent proteins at nanometer resolution. Science. 2006 Sep 15;313(5793):1642-5.

108. Chen F, Tillberg PW, Boyden ES. Optical imaging. Expansion microscopy. Science. 2015 Jan 30;347(6221):543-8.

109. Chozinski TJ, Halpern AR, Okawa H, Kim HJ, Tremel GJ, Wong RO, Vaughan JC. Expansion microscopy with conventional antibodies and fluorescent proteins. Nat Methods. 2016 Jun;13(6):485-8.

110. Sun DE, Fan X, Shi Y, Zhang H, Huang Z, Cheng B, Tang Q, Li W, Zhu Y, Bai J, Liu W, Li Y, Wang X, Lei X, Chen X. Click-ExM enables expansion microscopy for all biomolecules. Nat Methods. 2021 Jan;18(1):107-113.

111. Wen G, Vanheusden M, Acke A, Valli D, Neely RK, Leen V, Hofkens J. Evaluation of Direct Grafting Strategies via Trivalent Anchoring for Enabling Lipid Membrane and Cytoskeleton Staining in Expansion Microscopy. ACS Nano. 2020 Jul 28;14(7):7860-7867.

112. White BM, Kumar P, Conwell AN, Wu K, Baskin JM. Lipid Expansion Microscopy. J Am Chem Soc. 2022 Oct 12;144(40):18212-18217.

113. Sarkar D, Kang J, Wassie AT, Schroeder ME, Peng Z, Tarr TB, Tang AH, Niederst ED, Young JZ, Su H, Park D, Yin P, Tsai LH, Blanpied TA, Boyden ES. Revealing nanostructures in brain tissue via protein decrowding by iterative expansion microscopy. Nat Biomed Eng. 2022 Sep;6(9):1057-1073.